

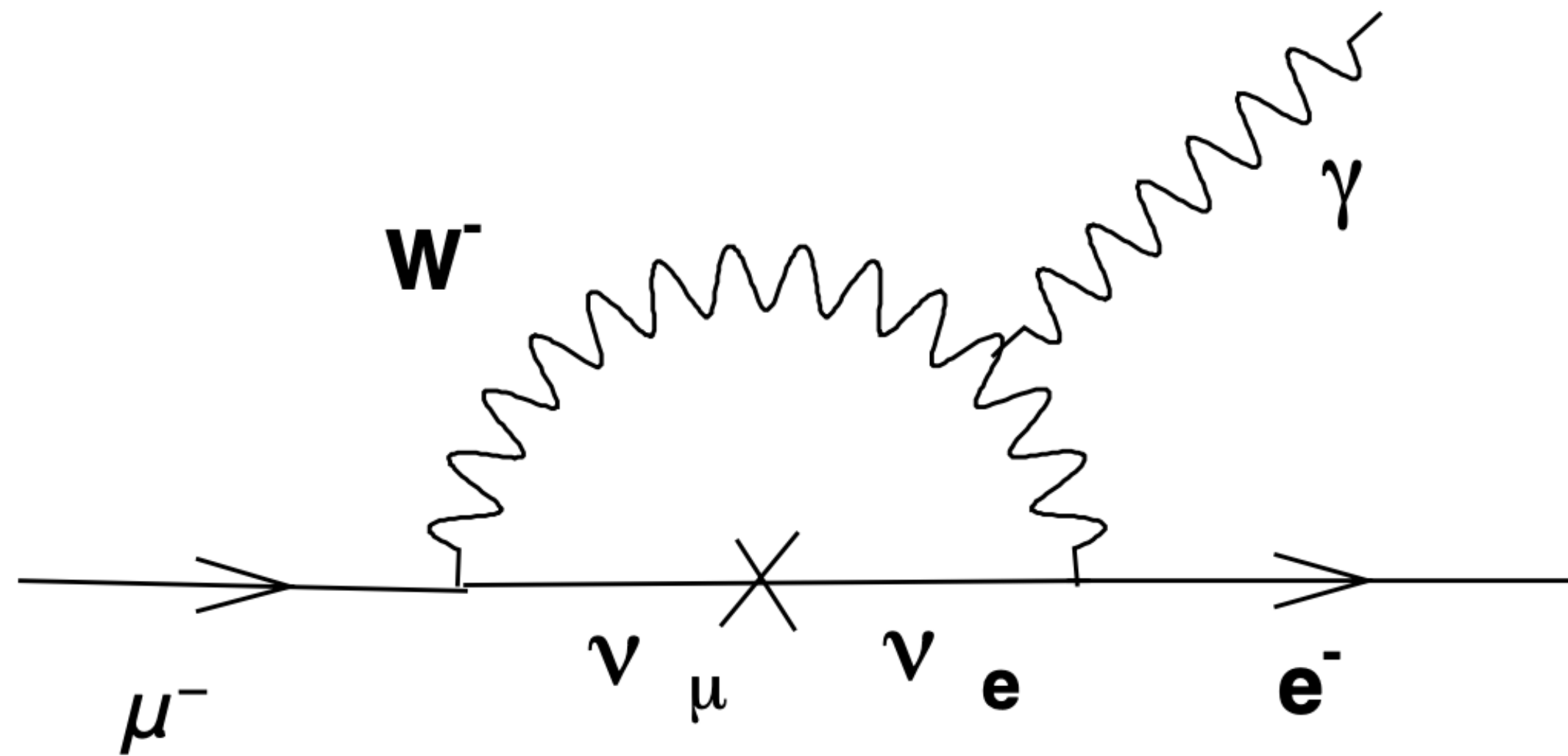
Probing Charged Lepton Flavor Violation with a Positron Beam at CEBAF

Sonny Mantry
University of North Georgia

In collaboration with Yulia Furletova
European Physical Journal A 57(315), 2021

Lepton Flavor Violation

- Discovery of neutrino oscillations indicate that neutrinos have mass!
- Neutrino oscillations imply Lepton Flavor Violation (LFV).
- LFV in the neutrinos also implies Charged Lepton Flavor Violation (CLFV):



However, the SM rate for CLFV is tiny due to small neutrino masses:

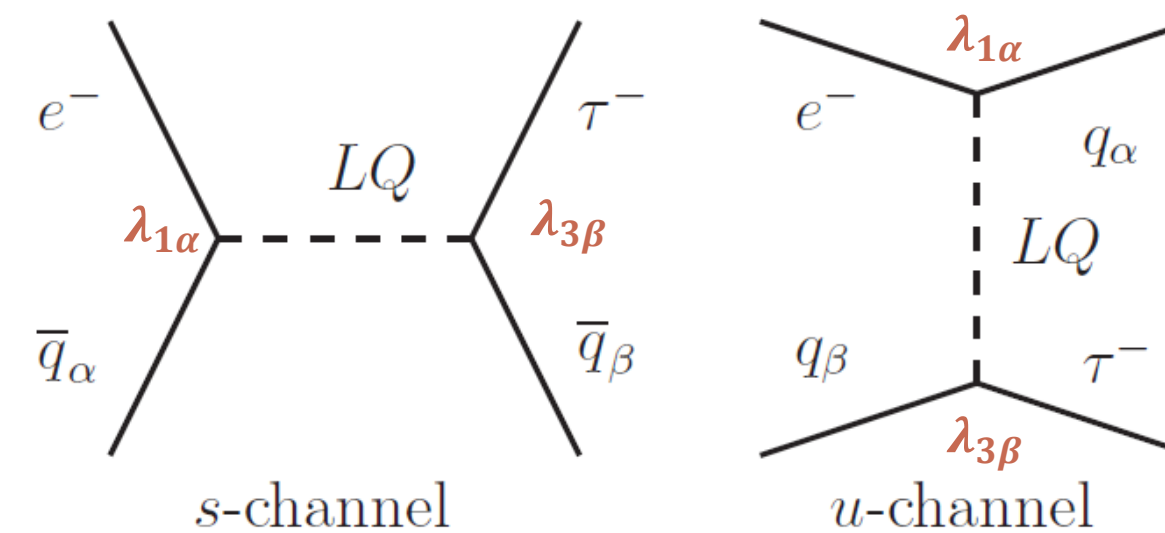
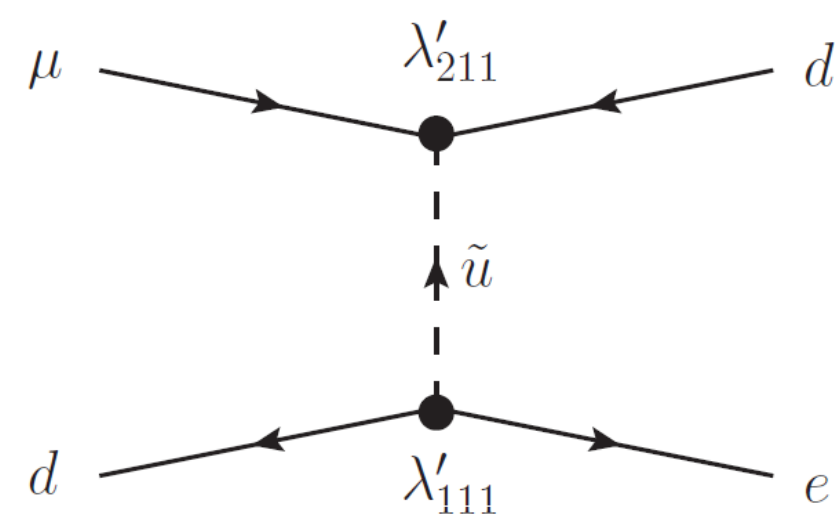
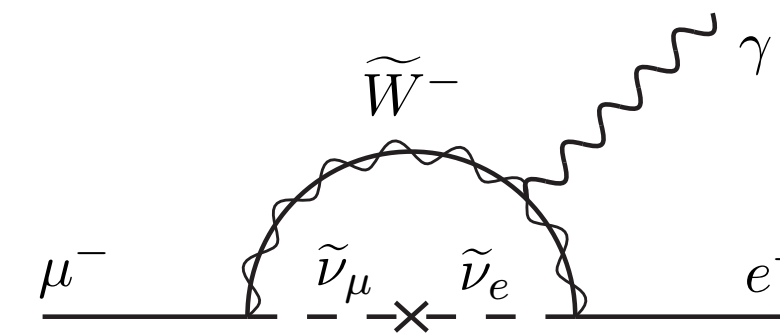
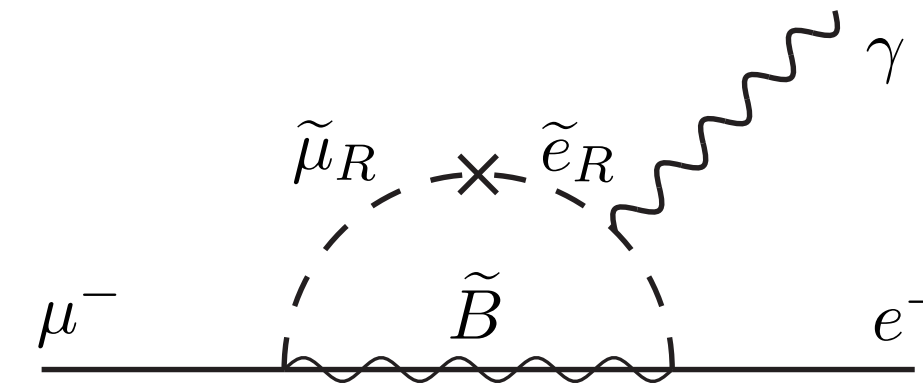
$$\text{BR}(\mu \rightarrow e\gamma) < 10^{-54}$$

- No hope of detecting such small rates for CLFV at any present or future planned experiments!

Lepton Flavor Violation in BSM

- However, many BSM scenarios predict enhanced CLFV rates:

- SUSY (RPV)
- SU(5), SO(10) GUTS
- Left-Right symmetric models
- Randall-Sundrum Models
- LeptoQuarks
- ...



- Leptoquarks can generate CLFV at tree level! Likely to produce enhanced CLFV rates compared to loop level processes in other models.

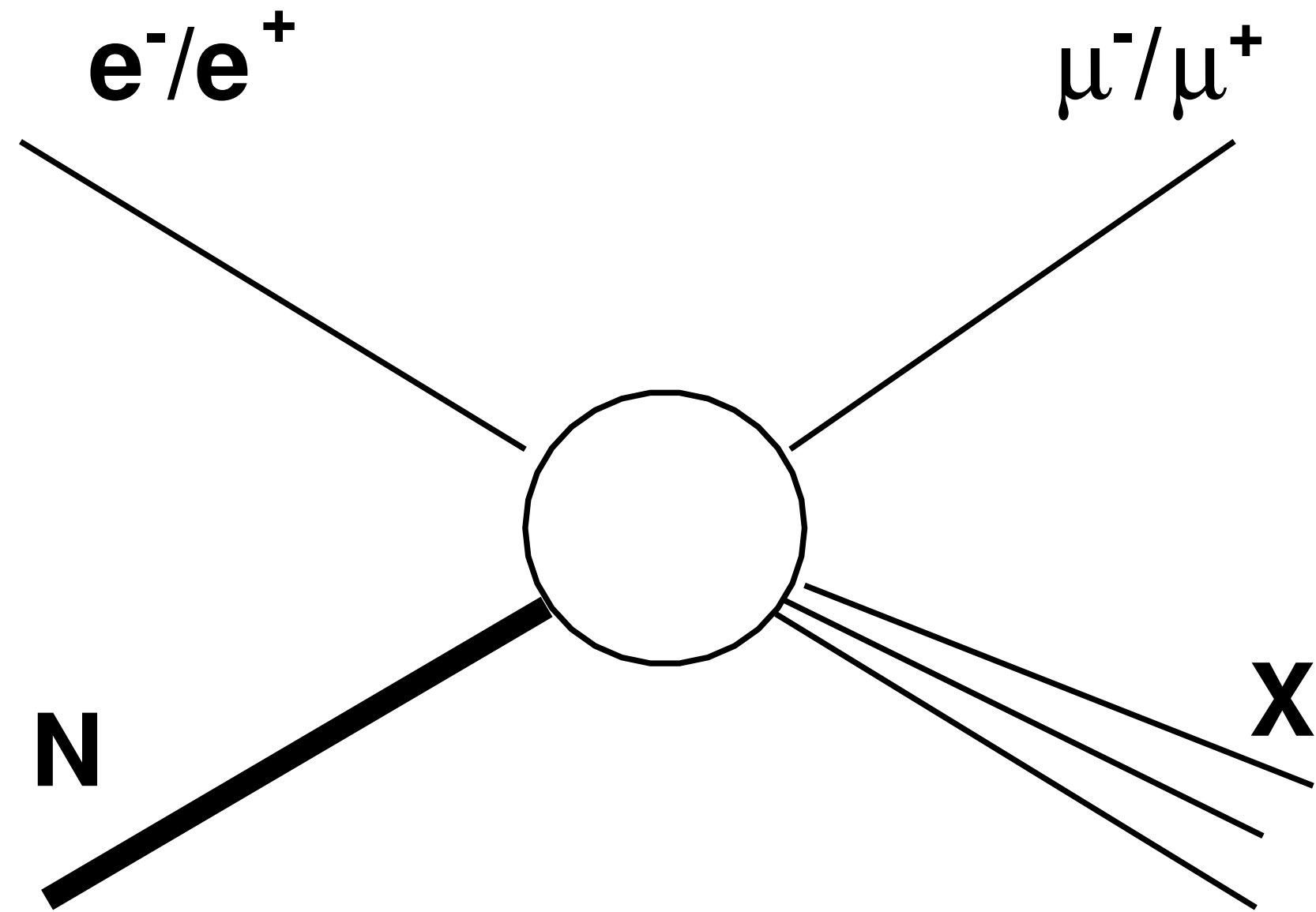
Charged Lepton Flavor Violation Limits

- Present and future limits:

Process	Experiment	Limit (90% <i>C. L.</i>)	Year
$\mu \rightarrow e\gamma$	MEGA	$Br < 1.2 \times 10^{-11}$	2002
$\mu + Au \rightarrow e + Au$	SINDRUM II	$\Gamma_{conv}/\Gamma_{capt} < 7.0 \times 10^{-13}$	2006
$\mu \rightarrow 3e$	SINDRUM	$Br < 1.0 \times 10^{-12}$	1988
$\tau \rightarrow e\gamma$	BaBar	$Br < 3.3 \times 10^{-8}$	2010
$\tau \rightarrow \mu\gamma$	BaBar	$Br < 6.8 \times 10^{-8}$	2005
$\tau \rightarrow 3e$	BELLE	$Br < 3.6 \times 10^{-8}$	2008
$\mu + N \rightarrow e + N$	Mu2e	$\Gamma_{conv}/\Gamma_{capt} < 6.0 \times 10^{-17}$	2017?
$\mu \rightarrow e\gamma$	MEG	$Br \lesssim 10^{-13}$	2011?
$\tau \rightarrow e\gamma$	Super-B	$Br \lesssim 10^{-10}$	> 2020?

- Note that CLFV(1,2) is severely constrained. Limits on CLFV(1,3) are weaker by several orders of magnitude.
- Limits on CLFV(1,2) are expected to improve even further in future experiments.

CLFV(1,2) in DIS



$$e^{\pm} + N \rightarrow \mu^{\pm} + X$$

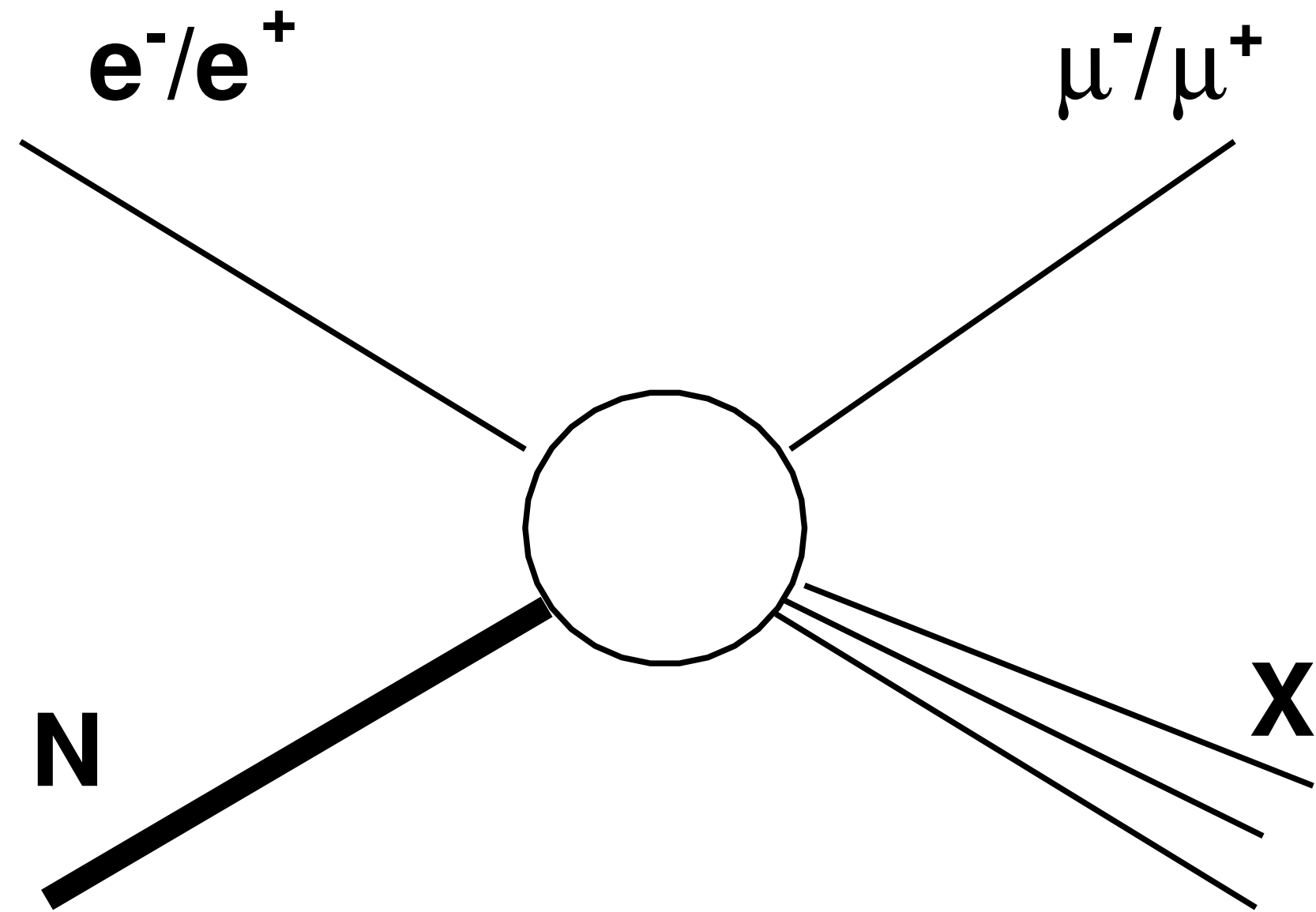
- One can also search for CLFV(1,2) in the DIS process, which can probe different CLFV mechanisms and is complementary to the other low energy experiments.
- There are already CLFV(1,2) limits from the *H1* and ZEUS collaborations at HERA. For example, the *H1* collaboration made searches for the settings: [S. Chekanov et.al (ZEUS), A. Atkas et.al (H1)]

$$\sqrt{s} = 319 \text{ GeV}$$

$$H1, e^-p : \mathcal{L} = 166 \text{ pb}^{-1}$$

$$H1, e^+p : \mathcal{L} = 245 \text{ pb}^{-1}$$

CLFV(1,2) in DIS



$$e^{\pm} + N \rightarrow \mu^{\pm} + X$$

- One can also set limits on CLFV(1,2) at JLAB:

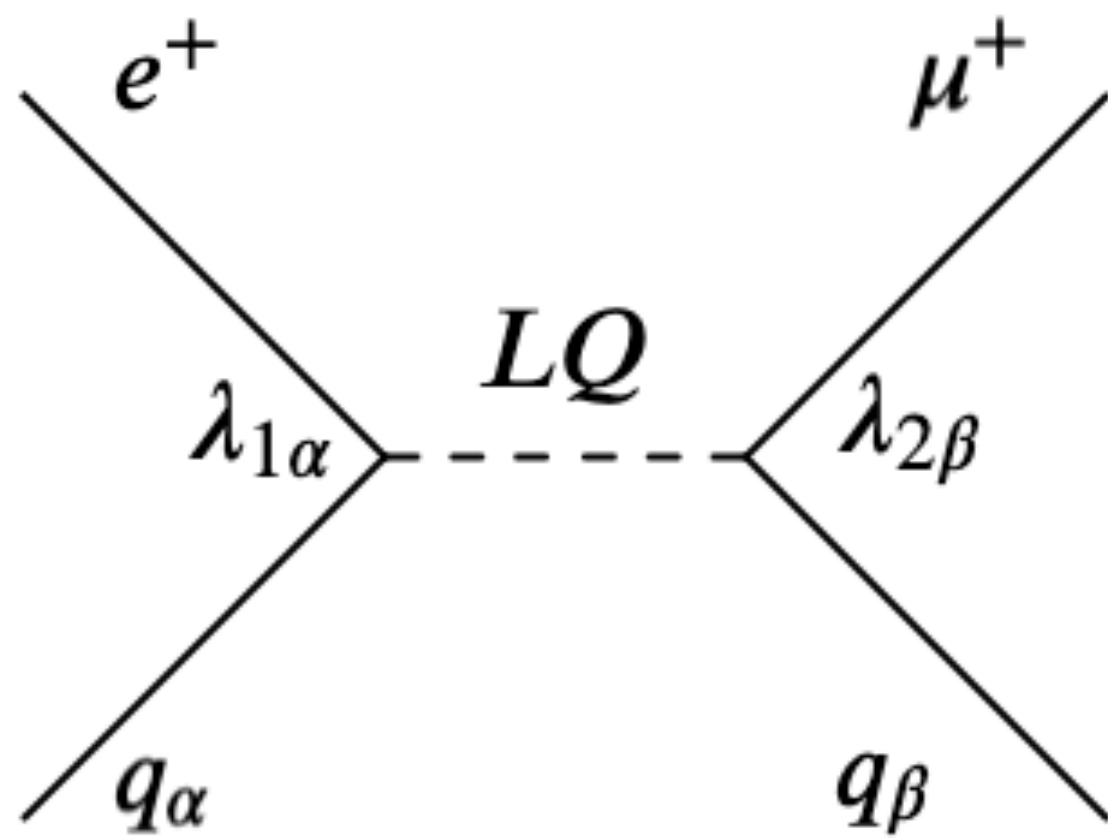
$$\sqrt{s} = 4.5 \text{ GeV}$$

$$\text{JLAB} : \mathcal{L} = 10^{36-39} \text{ cm}^{-2} \text{ s}^{-1}$$

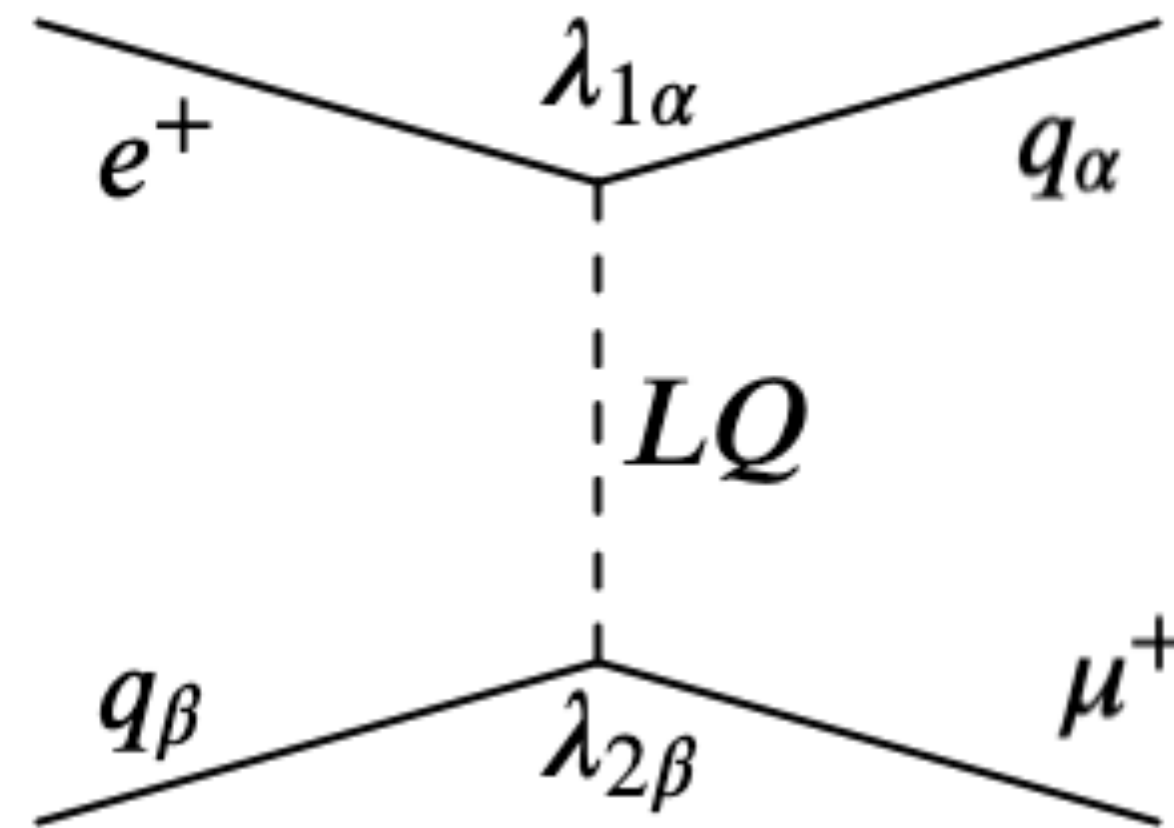
- Even though the center of mass energy is very small compared to HERA, corresponding to a much lower mass reach, the much larger luminosity could allow for improvement over HERA by up to two orders of magnitude.

CLFV Mediated by Leptoquarks

$$e^{\pm} + N \rightarrow \mu^{\pm} + X$$

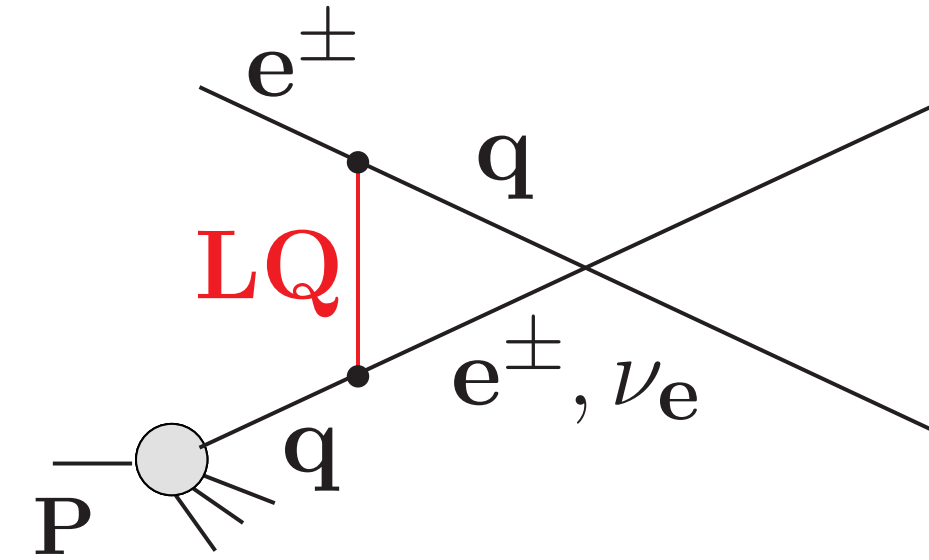
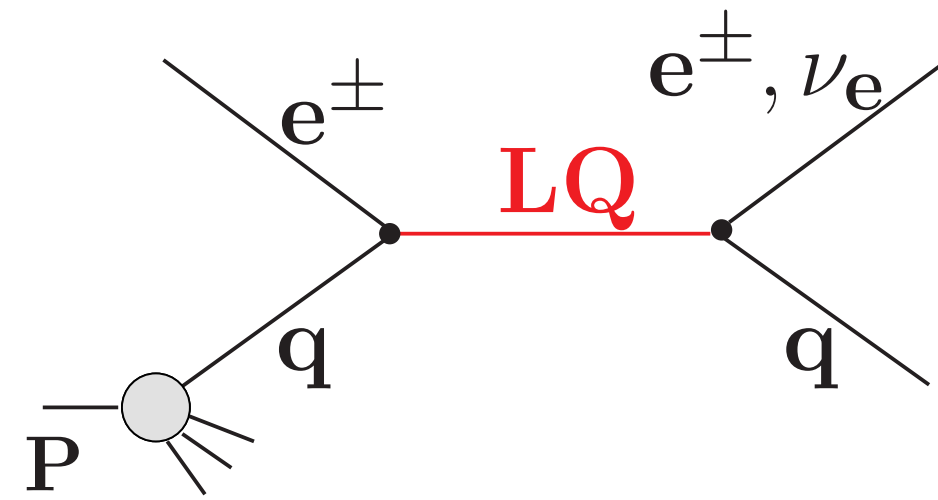


s-channel Leptoquark exchange



t-channel Leptoquark exchange

Leptoquarks



- Leptoquarks (LQs) are color triplet bosons that couple leptons to quarks
- LQs arise in many BSM models:
 - Pati-Salam Model
 - GUTs: SU(5), SO(10),...
 - Extended Technicolor
- LQs have a rich phenomenology and come in 14 types, classified according to:
 - Fermion number $F=3B+L$ [$|F|=0, 2$]
 - Spin [scalar (S) or vector (V)]
 - Chirality of coupling to leptons [L or R]
 - Gauge group quantum numbers [$SU(2)_L \times U(1)_Y$]

Leptoquarks

- Renormalizable and gauge invariant couplings of LQs to quarks and leptons:

$$\mathcal{L}_{F=0} = h_{1/2}^L \bar{u}_R \ell_L S_{1/2}^L + h_{1/2}^R \bar{q}_L \epsilon e_R S_{1/2}^R + \tilde{h}_{1/2}^L \bar{d}_R \ell_L \tilde{S}_{1/2}^L + h_0^L \bar{q}_L \gamma_\mu \ell_L V_0^{L\mu} \\ + h_0^R \bar{d}_R \gamma_\mu e_R V_0^{R\mu} + \tilde{h}_0^R \bar{u}_R \gamma_\mu e_R \tilde{V}_0^{R\mu} + h_1^L \bar{q}_L \gamma_\mu \vec{\tau} \ell_L \vec{V}_1^{L\mu} + \text{h.c.}$$

$$\mathcal{L}_{|F|=2} = g_0^L \bar{q}_L^c \epsilon \ell_L S_0^L + g_0^R \bar{u}_R^c e_R S_0^R + \tilde{g}_0^R \bar{d}_R^c e_R \tilde{S}_0^R + g_1^L \bar{q}_L^c \epsilon \vec{\tau} \ell_L \vec{S}_1^L + g_{1/2}^L \bar{d}_R^c \gamma_\mu \ell_L V_{1/2}^{L\mu} \\ + g_{1/2}^R \bar{q}_L^c \gamma_\mu e_R V_{1/2}^{R\mu} + \tilde{g}_{1/2}^L \bar{u}_R^c \gamma_\mu \ell_L \tilde{V}_{1/2}^{L\mu} + \text{h.c.}$$

- Classification of the 14 types of LQs: [Buchmuller, Ruckl, Wyler (BRW)]

Type	J	F	Q	ep dominant process	Coupling	Branching ratio β_ℓ	Type	J	F	Q	ep dominant process	Coupling	Branching ratio β_ℓ
S_0^L	0	2	-1/3	$e_L^- u_L \rightarrow \begin{cases} \ell^- u \\ \nu_\ell d \end{cases}$	$\begin{matrix} \lambda_L \\ -\lambda_L \end{matrix}$	$\begin{matrix} 1/2 \\ 1/2 \end{matrix}$	V_0^L	1	0	+2/3	$e_R^+ d_L \rightarrow \begin{cases} \ell^+ d \\ \bar{\nu}_\ell u \end{cases}$	$\begin{matrix} \lambda_L \\ \lambda_L \end{matrix}$	$\begin{matrix} 1/2 \\ 1/2 \end{matrix}$
S_0^R	0	2	-1/3	$e_R^- u_R \rightarrow \ell^- u$	λ_R	1	V_0^R	1	0	+2/3	$e_L^+ d_R \rightarrow \ell^+ d$	λ_R	1
\tilde{S}_0^R	0	2	-4/3	$e_R^- d_R \rightarrow \ell^- d$	λ_R	1	\tilde{V}_0^R	1	0	+5/3	$e_L^+ u_R \rightarrow \ell^+ u$	λ_R	1
S_1^L	0	2	-1/3	$e_L^- u_L \rightarrow \begin{cases} \ell^- u \\ \nu_\ell d \end{cases}$	$\begin{matrix} -\lambda_L \\ -\lambda_L \end{matrix}$	$\begin{matrix} 1/2 \\ 1/2 \end{matrix}$	V_1^L	1	0	+2/3	$e_R^+ d_L \rightarrow \begin{cases} \ell^+ d \\ \bar{\nu}_\ell u \end{cases}$	$\begin{matrix} -\lambda_L \\ \lambda_L \end{matrix}$	$\begin{matrix} 1/2 \\ 1/2 \end{matrix}$
			-4/3	$e_L^- d_L \rightarrow \ell^- d$	$-\sqrt{2}\lambda_L$	1							+5/3
$V_{1/2}^L$	1	2	-4/3	$e_L^- d_R \rightarrow \ell^- d$	λ_L	1	$S_{1/2}^L$	0	0	+5/3	$e_R^+ u_R \rightarrow \ell^+ u$	λ_L	1
$V_{1/2}^R$	1	2	-1/3	$e_R^- u_L \rightarrow \ell^- u$	λ_R	1	$S_{1/2}^R$	0	0	+2/3	$e_L^+ d_L \rightarrow \ell^+ d$	$-\lambda_R$	1
			-4/3	$e_R^- d_L \rightarrow \ell^- d$	λ_R	1				+5/3	$e_L^+ u_L \rightarrow \ell^+ u$	λ_R	1
$\tilde{V}_{1/2}^L$	1	2	-1/3	$e_L^- u_R \rightarrow \ell^- u$	λ_L	1	$\tilde{S}_{1/2}^L$	0	0	+2/3	$e_R^+ d_R \rightarrow \ell^+ d$	λ_L	1

Leptoquarks

[Buchmuller, Ruckl, Wyler (BRW)]

Type	J	F	Q	ep dominant process	Coupling	Branching ratio β_ℓ	Type	J	F	Q	ep dominant process	Coupling	Branching ratio β_ℓ
S_0^L	0	2	-1/3	$e_L^- u_L \rightarrow \begin{cases} \ell^- u \\ \nu_\ell d \end{cases}$	$\begin{matrix} \lambda_L \\ -\lambda_L \end{matrix}$	$\begin{matrix} 1/2 \\ 1/2 \end{matrix}$	V_0^L	1	0	+2/3	$e_R^+ d_L \rightarrow \begin{cases} \ell^+ d \\ \bar{\nu}_\ell u \end{cases}$	$\begin{matrix} \lambda_L \\ \lambda_L \end{matrix}$	$\begin{matrix} 1/2 \\ 1/2 \end{matrix}$
S_0^R	0	2	-1/3	$e_R^- u_R \rightarrow \ell^- u$	λ_R	1	V_0^R	1	0	+2/3	$e_L^+ d_R \rightarrow \ell^+ d$	λ_R	1
\tilde{S}_0^R	0	2	-4/3	$e_R^- d_R \rightarrow \ell^- d$	λ_R	1	\tilde{V}_0^R	1	0	+5/3	$e_L^+ u_R \rightarrow \ell^+ u$	λ_R	1
S_1^L	0	2	-1/3	$e_L^- u_L \rightarrow \begin{cases} \ell^- u \\ \nu_\ell d \end{cases}$	$\begin{matrix} -\lambda_L \\ -\lambda_L \end{matrix}$	$\begin{matrix} 1/2 \\ 1/2 \end{matrix}$	V_1^L	1	0	+2/3	$e_R^+ d_L \rightarrow \begin{cases} \ell^+ d \\ \bar{\nu}_\ell u \end{cases}$	$\begin{matrix} -\lambda_L \\ \lambda_L \end{matrix}$	$\begin{matrix} 1/2 \\ 1/2 \end{matrix}$
			-4/3	$e_L^- d_L \rightarrow \ell^- d$	$-\sqrt{2}\lambda_L$	1				+5/3	$e_R^+ u_L \rightarrow \ell^+ u$	$\sqrt{2}\lambda_L$	1
$V_{1/2}^L$	1	2	-4/3	$e_L^- d_R \rightarrow \ell^- d$	λ_L	1	$S_{1/2}^L$	0	0	+5/3	$e_R^+ u_R \rightarrow \ell^+ u$	λ_L	1
$V_{1/2}^R$	1	2	-1/3	$e_R^- u_L \rightarrow \ell^- u$	λ_R	1	$S_{1/2}^R$	0	0	+2/3	$e_L^+ d_L \rightarrow \ell^+ d$	$-\lambda_R$	1
			-4/3	$e_R^- d_L \rightarrow \ell^- d$	λ_R	1				+5/3	$e_L^+ u_L \rightarrow \ell^+ u$	λ_R	1
$\tilde{V}_{1/2}^L$	1	2	-1/3	$e_L^- u_R \rightarrow \ell^- u$	λ_L	1	$\tilde{S}_{1/2}^L$	0	0	+2/3	$e_R^+ d_R \rightarrow \ell^+ d$	λ_L	1

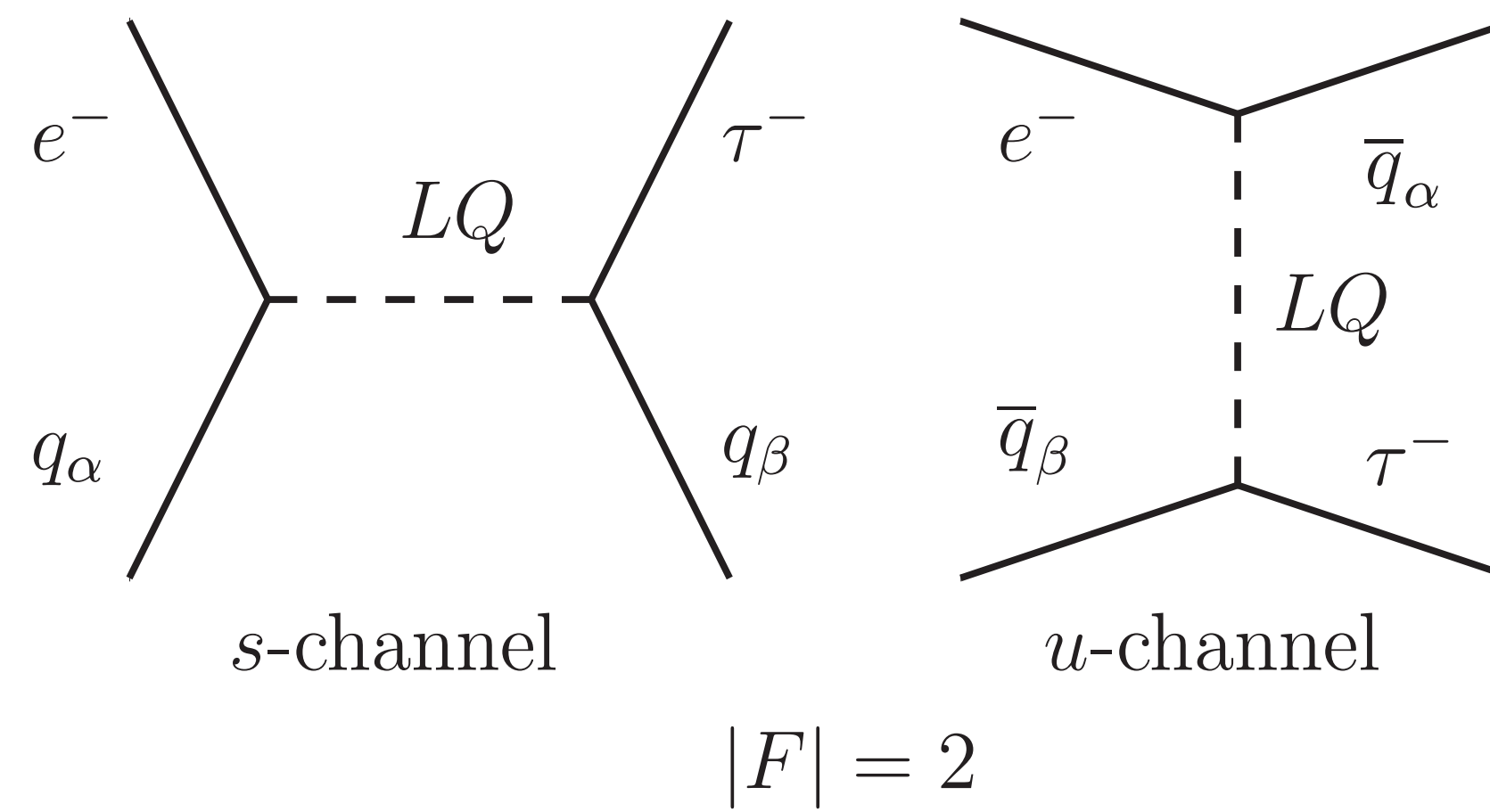
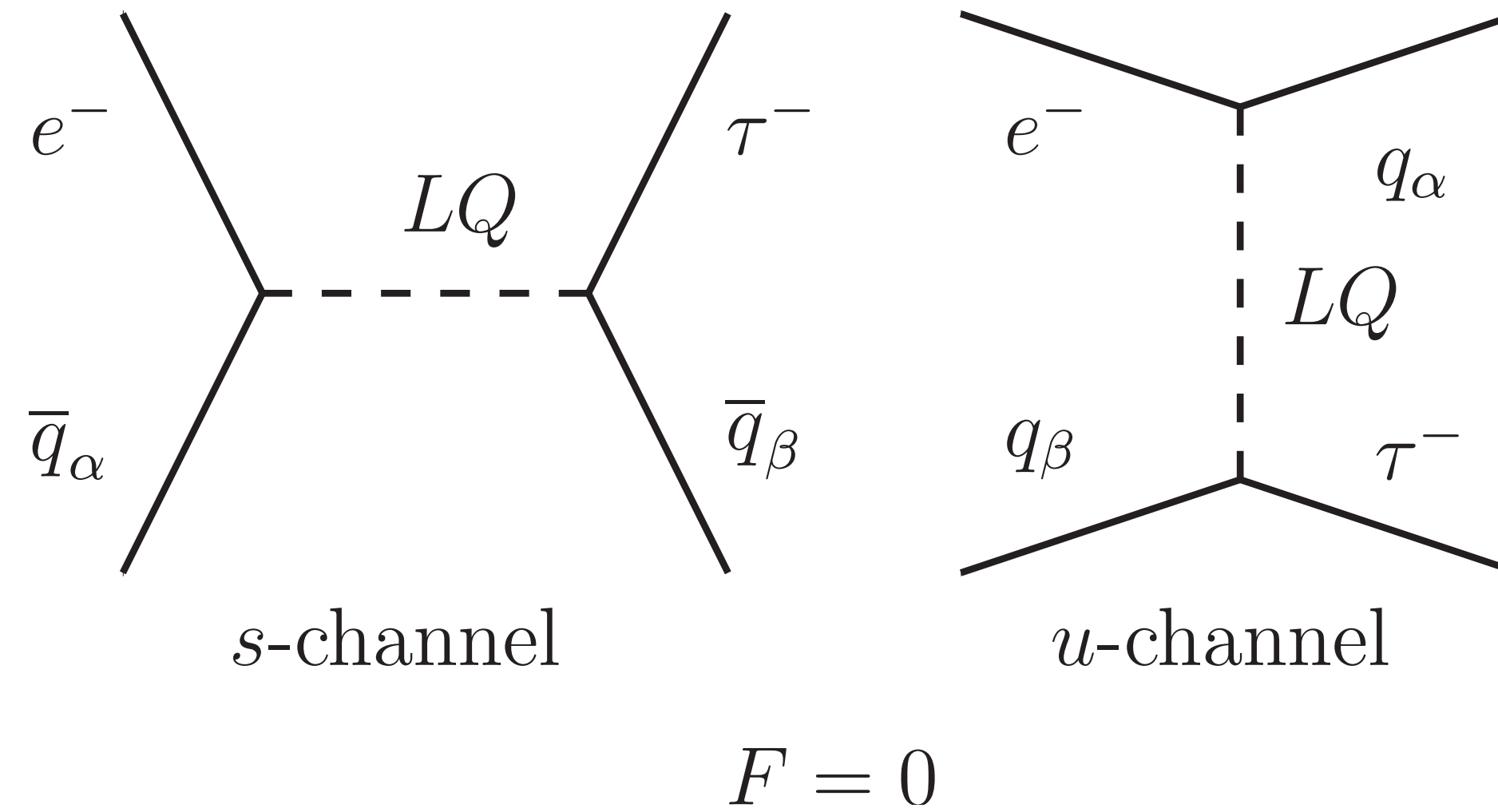
- In order to maximally exploit the phenomenology of LQs and be able to distinguish between different types of LQ states, we need:

- electron and positron beams
- proton and deuteron targets
- polarized beams
- wide kinematic range

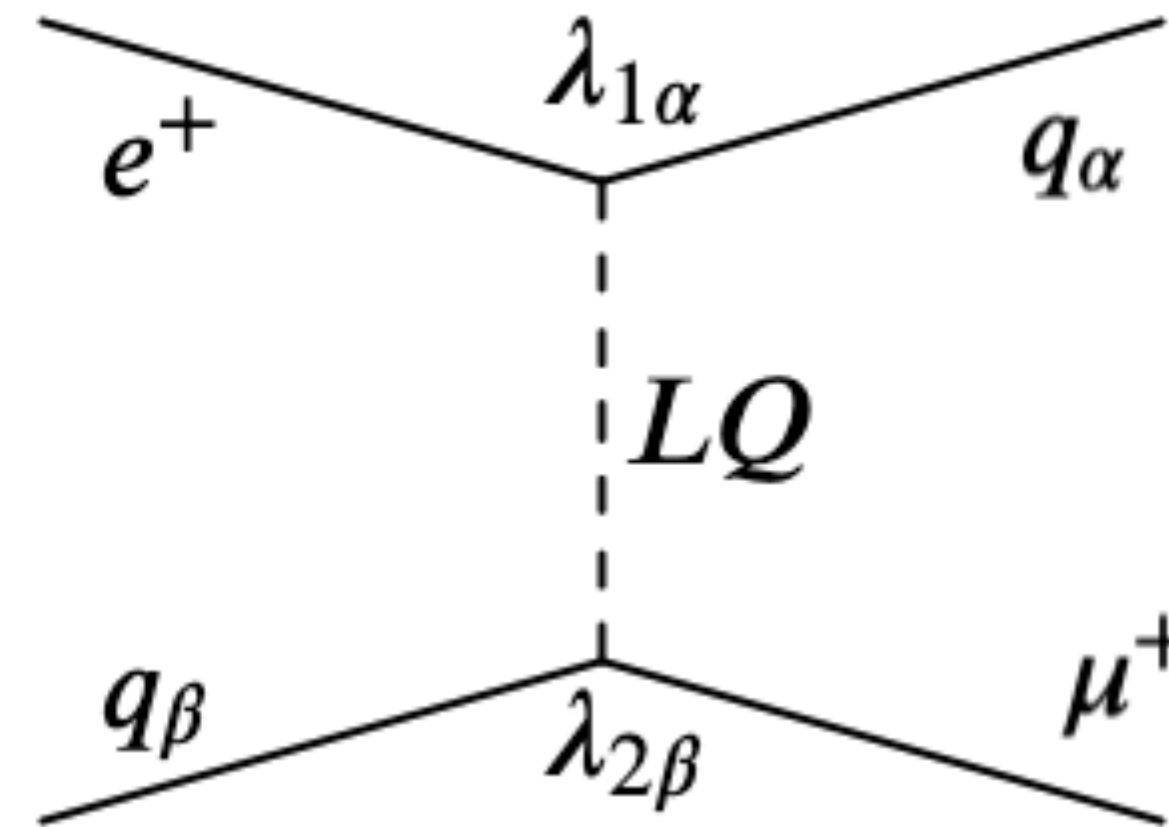
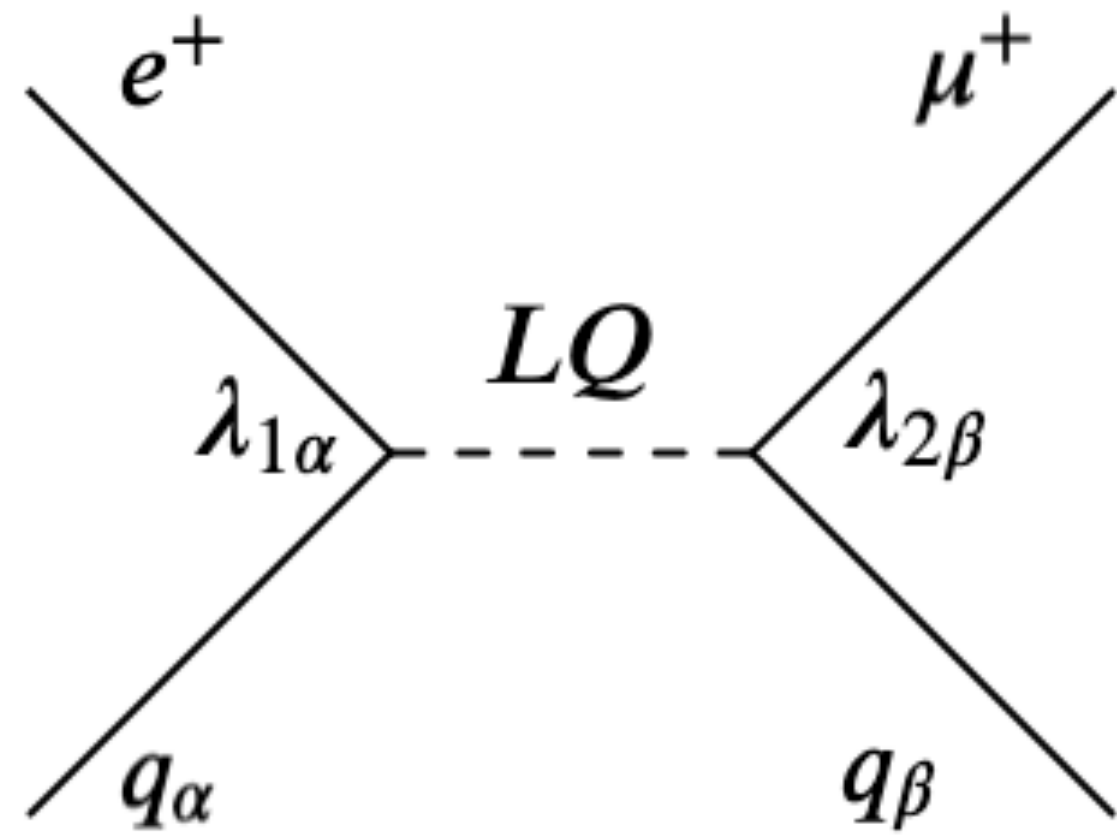
- [separate $|F|=0$ vs $|F|=2$]
- [separate “eu” vs “ed” LQs]
- [separate L vs R]
- [separate scalar vs vector LQs]

F=0 vs. |F|=2 Leptoquarks

$$F = 3B + L$$



Tree-Level Cross Sections For Leptoquark Mediated CLFV



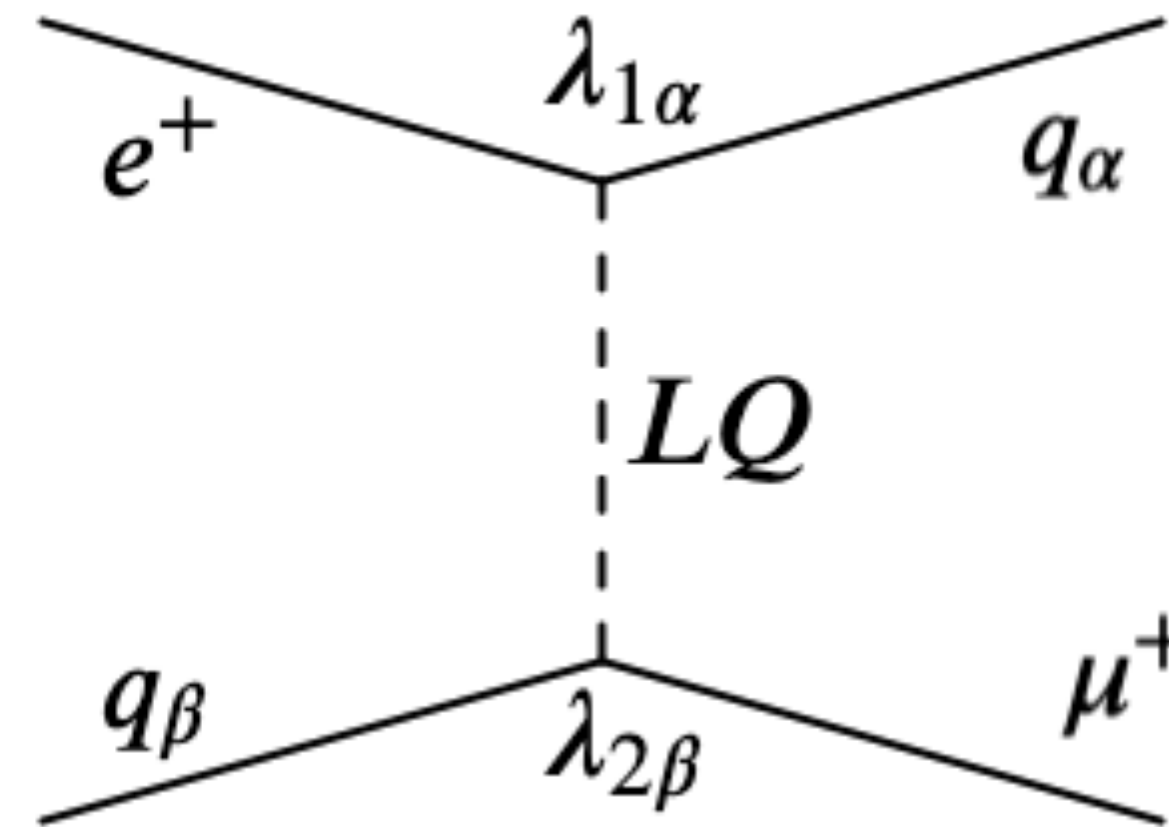
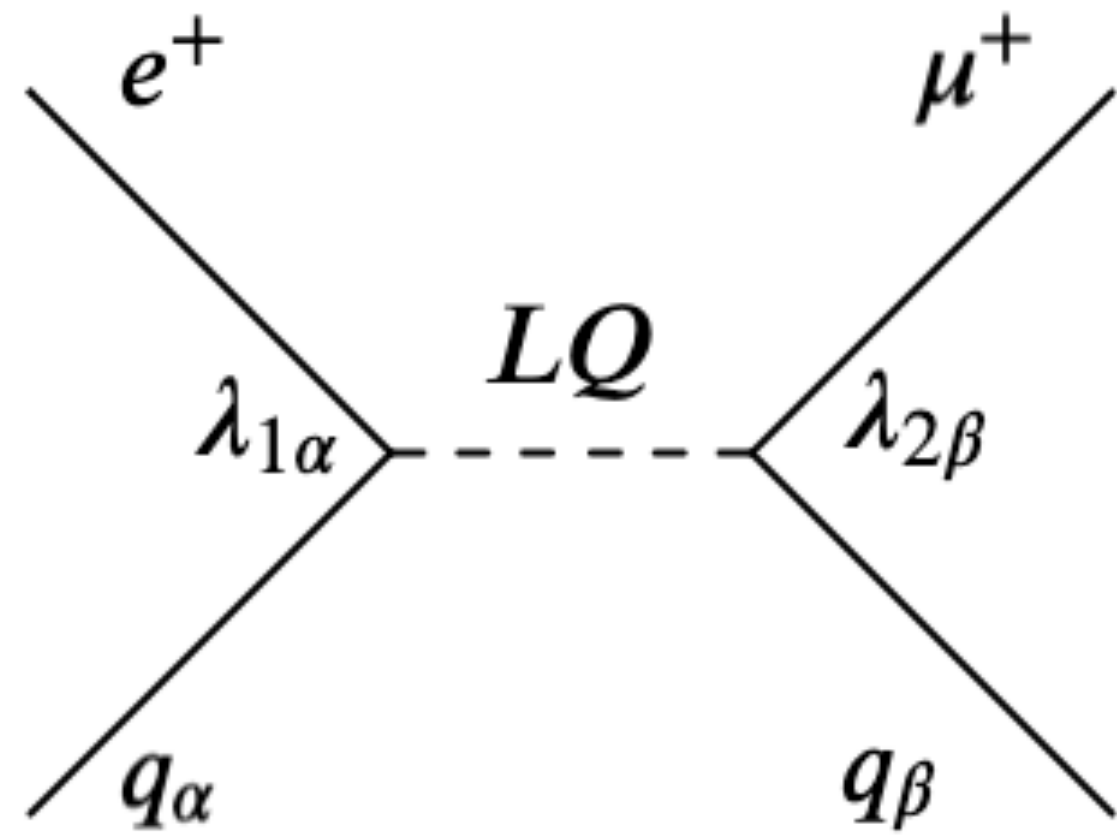
$$\sigma_{F=0}^{e^+p} = \sum_{\alpha,\beta} \frac{s}{32\pi} \left[\frac{\lambda_{1\alpha}\lambda_{2\beta}}{M_{LQ}^2} \right]^2 \int dx \int dy \left\{ xq_{\alpha}(x, xs)f(y) + x\bar{q}_{\beta}(x, -u)g(y) \right\}$$

$$\sigma_{|F|=2}^{e^+p} = \sum_{\alpha,\beta} \frac{s}{32\pi} \left[\frac{\lambda_{1\alpha}\lambda_{2\beta}}{M_{LQ}^2} \right]^2 \int dx \int dy \left\{ x\bar{q}_{\alpha}(x, xs)f(y) + q_{\beta}(x, -u)g(y) \right\}$$

$$f(y) = \begin{cases} 1/2 & \text{(scalar)} \\ 2(1-y)^2 & \text{(vector)} \end{cases}, \quad g(y) = \begin{cases} (1-y)^2/2 & \text{(scalar)} \\ 2 & \text{(vector)} \end{cases}$$

Comparing limits from obtained from electron vs. positron beams can help disentangle contributions from $F=0$ vs. $|F|=2$ leptoquarks due to different combinations of quark or antiquark PDFs arising in the s- and u-channels.

Tree-Level Cross Sections For Leptoquark Mediated CLFV



$$\sigma_{F=0}^{e^+p} = \sum_{\alpha,\beta} \frac{s}{32\pi} \left[\frac{\lambda_{1\alpha}\lambda_{2\beta}}{M_{LQ}^2} \right]^2 \int dx \int dy \left\{ x q_\alpha(x, xs) f(y) + x \bar{q}_\beta(x, -u) g(y) \right\}$$

$$\sigma_{|F|=2}^{e^+p} = \sum_{\alpha,\beta} \frac{s}{32\pi} \left[\frac{\lambda_{1\alpha}\lambda_{2\beta}}{M_{LQ}^2} \right]^2 \int dx \int dy \left\{ x \bar{q}_\alpha(x, xs) f(y) + q_\beta(x, -u) g(y) \right\}$$

$$f(y) = \begin{cases} 1/2 & \text{(scalar)} \\ 2(1-y)^2 & \text{(vector)} \end{cases}, \quad g(y) = \begin{cases} (1-y)^2/2 & \text{(scalar)} \\ 2 & \text{(vector)} \end{cases}$$

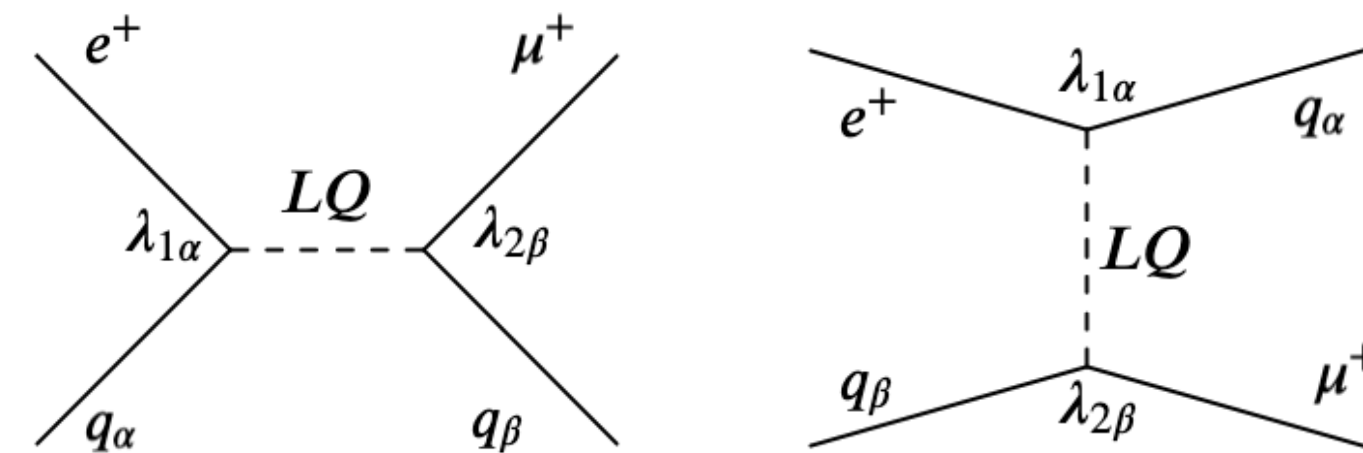
Tree-Level Cross Sections For Leptoquark Mediated CLFV

$$\sigma_{F=0}^{e^+p} = \sum_{\alpha,\beta} \frac{s}{32\pi} \left[\frac{\lambda_{1\alpha}\lambda_{2\beta}}{M_{LQ}^2} \right]^2 \int dx \int dy \left\{ xq_\alpha(x, xs)f(y) + x\bar{q}_\beta(x, -u)g(y) \right\}$$

$$\sigma_{|F|=2}^{e^+p} = \sum_{\alpha,\beta} \frac{s}{32\pi} \left[\frac{\lambda_{1\alpha}\lambda_{2\beta}}{M_{LQ}^2} \right]^2 \int dx \int dy \left\{ x\bar{q}_\alpha(x, xs)f(y) + q_\beta(x, -u)g(y) \right\}$$

- Limits can be set on the contact interaction factor:

$$\chi_{\alpha\beta} \equiv \frac{\lambda_{1\alpha}\lambda_{2\beta}}{M_{LQ}^2}$$



- It becomes useful to define the ratio of the contact interaction factor to its HERA limit. The cross section can now be thought of as a function of z :

$$z \equiv \frac{\chi_{\alpha\beta}}{\chi_{\alpha\beta}^{\text{HERA}}}$$

- Any obtained limit of $z < 1$, would signal an improvement over the HERA limit.

Preliminary Estimate of CLFV Limits with a Positron Beam at JLAB

Type	J	F	Q	ep dominant process	Coupling	Branching ratio β_ℓ	Type	J	F	Q	ep dominant process	Coupling	Branching ratio β_ℓ
S_0^L	0	2	-1/3	$e_L^- u_L \rightarrow \begin{cases} \ell^- u \\ \nu_\ell d \end{cases}$	$\begin{matrix} \lambda_L \\ -\lambda_L \end{matrix}$	$\begin{matrix} 1/2 \\ 1/2 \end{matrix}$	V_0^L	1	0	+2/3	$e_R^+ d_L \rightarrow \begin{cases} \ell^+ d \\ \bar{\nu}_\ell u \end{cases}$	$\begin{matrix} \lambda_L \\ \lambda_L \end{matrix}$	$\begin{matrix} 1/2 \\ 1/2 \end{matrix}$
S_0^R	0	2	-1/3	$e_R^- u_R \rightarrow \ell^- u$	λ_R	1	V_0^R	1	0	+2/3	$e_L^+ d_R \rightarrow \ell^+ d$	λ_R	1
\tilde{S}_0^R	0	2	-4/3	$e_R^- d_R \rightarrow \ell^- d$	λ_R	1	\tilde{V}_0^R	1	0	+5/3	$e_L^+ u_R \rightarrow \ell^+ u$	λ_R	1
S_1^L	0	2	-1/3	$e_L^- u_L \rightarrow \begin{cases} \ell^- u \\ \nu_\ell d \end{cases}$	$\begin{matrix} -\lambda_L \\ -\lambda_L \end{matrix}$	$\begin{matrix} 1/2 \\ 1/2 \end{matrix}$	V_1^L	1	0	+2/3	$e_R^+ d_L \rightarrow \begin{cases} \ell^+ d \\ \bar{\nu}_\ell u \end{cases}$	$\begin{matrix} -\lambda_L \\ \lambda_L \end{matrix}$	$\begin{matrix} 1/2 \\ 1/2 \end{matrix}$
			-4/3	$e_L^- d_L \rightarrow \ell^- d$	$-\sqrt{2}\lambda_L$	1				+5/3	$e_R^+ u_L \rightarrow \ell^+ u$	$\sqrt{2}\lambda_L$	1
$V_{1/2}^L$	1	2	-4/3	$e_L^- d_R \rightarrow \ell^- d$	λ_L	1	$S_{1/2}^L$	0	0	+5/3	$e_R^+ u_R \rightarrow \ell^+ u$	λ_L	1
$V_{1/2}^R$	1	2	-1/3	$e_R^- u_L \rightarrow \ell^- u$	λ_R	1	$S_{1/2}^R$	0	0	+2/3	$e_L^+ d_L \rightarrow \ell^+ d$	$-\lambda_R$	1
			-4/3	$e_R^- d_L \rightarrow \ell^- d$	λ_R	1				+5/3	$e_L^+ u_L \rightarrow \ell^+ u$	λ_R	1
$\tilde{V}_{1/2}^L$	1	2	-1/3	$e_L^- u_R \rightarrow \ell^- u$	λ_L	1	$\tilde{S}_{1/2}^L$	0	0	+2/3	$e_R^+ d_R \rightarrow \ell^+ d$	λ_L	1

- Limits based on running for 5 years with instantaneous luminosity of $\mathcal{L} \sim 10^{38} \text{ cm}^{-2} \text{ s}^{-1}$

- Thus, JLAB could improve on HERA limits by two or three orders of magnitude: $z \sim [0.005 - 0.05]$

- This estimate will be modified after taking into account acceptance and background effects.

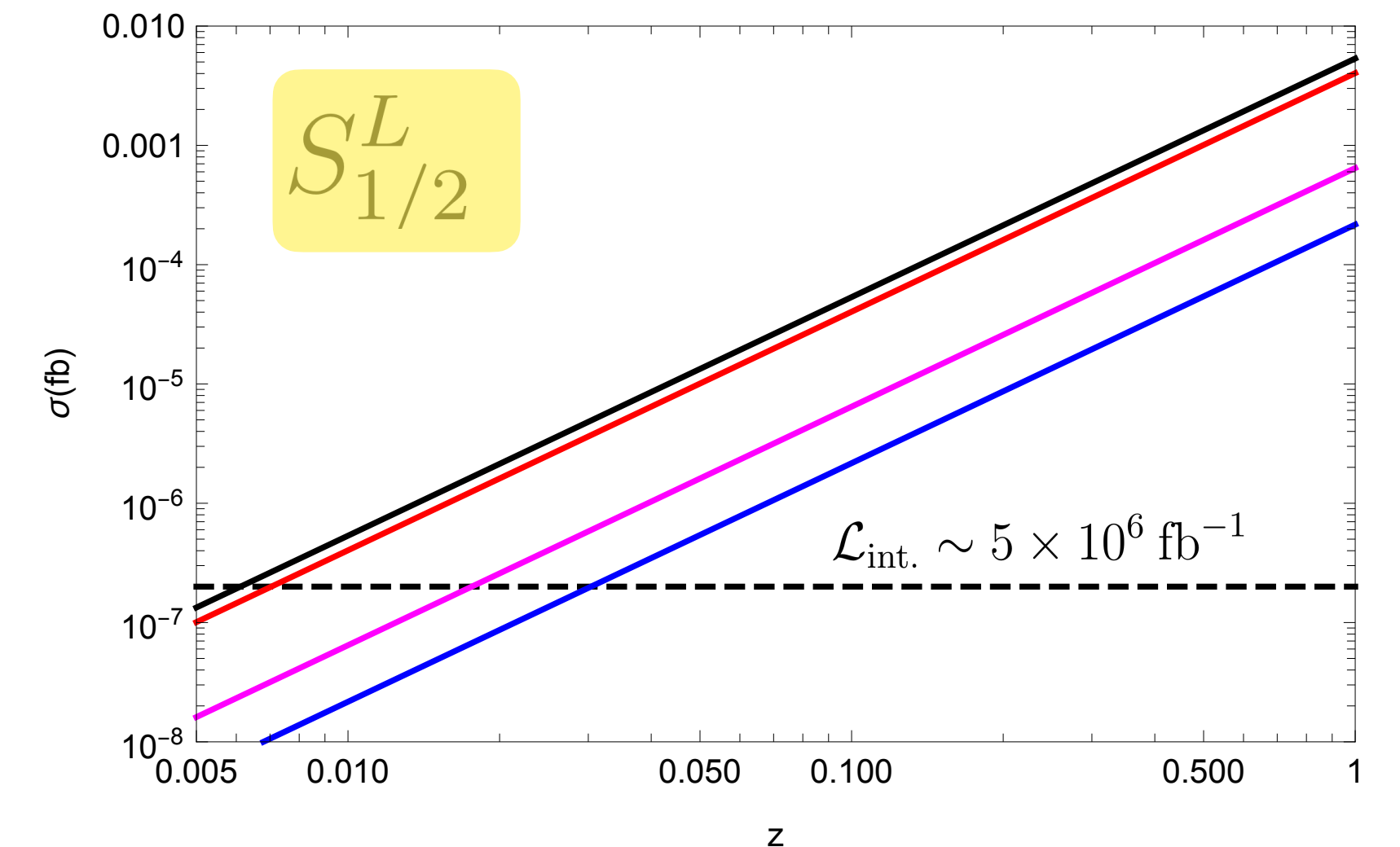


Fig. 5. The cross section for $e^+ N \rightarrow \mu^+ X$ with center of mass energy $\sqrt{s} = 4.5 \text{ GeV}$, via exchange of the $F=0$ scalar LQ, $S_{1/2}^L$, as a function of the ratio z defined in Eq. (9). The red, black, magenta, and blue solid lines correspond to the choices $(\alpha, \beta) = \{11, 12, 21, 22\}$ in Eq. (6) with all other terms set to zero. An integrated luminosity of $\mathcal{L} \sim 5 \times 10^6 \text{ fb}^{-1}$ will allow sensitivity to cross sections as small as $\sigma \sim 0.2 \times 10^{-6} \text{ fb}$ (horizontal dashed line).

Beam polarization dependence on CLFV Limits

Type	J	F	Q	ep dominant process	Coupling	Branching ratio β_ℓ	Type	J	F	Q	ep dominant process	Coupling	Branching ratio β_ℓ
S_0^L	0	2	-1/3	$e_L^- u_L \rightarrow \begin{cases} \ell^- u \\ \nu_\ell d \end{cases}$	$\begin{matrix} \lambda_L \\ -\lambda_L \end{matrix}$	$\begin{matrix} 1/2 \\ 1/2 \end{matrix}$	V_0^L	1	0	+2/3	$e_R^+ d_L \rightarrow \begin{cases} \ell^+ d \\ \bar{\nu}_\ell u \end{cases}$	$\begin{matrix} \lambda_L \\ \lambda_L \end{matrix}$	$\begin{matrix} 1/2 \\ 1/2 \end{matrix}$
S_0^R	0	2	-1/3	$e_R^- u_R \rightarrow \ell^- u$	λ_R	1	V_0^R	1	0	+2/3	$e_L^+ d_R \rightarrow \ell^+ d$	λ_R	1
\tilde{S}_0^R	0	2	-4/3	$e_R^- d_R \rightarrow \ell^- d$	λ_R	1	\tilde{V}_0^R	1	0	+5/3	$e_L^+ u_R \rightarrow \ell^+ u$	λ_R	1
S_1^L	0	2	-1/3	$e_L^- u_L \rightarrow \begin{cases} \ell^- u \\ \nu_\ell d \end{cases}$	$\begin{matrix} -\lambda_L \\ -\lambda_L \end{matrix}$	$\begin{matrix} 1/2 \\ 1/2 \end{matrix}$	V_1^L	1	0	+2/3	$e_R^+ d_L \rightarrow \begin{cases} \ell^+ d \\ \bar{\nu}_\ell u \end{cases}$	$\begin{matrix} -\lambda_L \\ \lambda_L \end{matrix}$	$\begin{matrix} 1/2 \\ 1/2 \end{matrix}$
			-4/3	$e_L^- d_L \rightarrow \ell^- d$	$-\sqrt{2}\lambda_L$	1				+5/3	$e_R^+ u_L \rightarrow \ell^+ u$	$\sqrt{2}\lambda_L$	1
$V_{1/2}^L$	1	2	-4/3	$e_L^- d_R \rightarrow \ell^- d$	λ_L	1	$S_{1/2}^L$	0	0	+5/3	$e_R^+ u_R \rightarrow \ell^+ u$	λ_L	1
$V_{1/2}^R$	1	2	-1/3	$e_R^- u_L \rightarrow \ell^- u$	λ_R	1	$S_{1/2}^R$	0	0	+2/3	$e_L^+ d_L \rightarrow \ell^+ d$	$-\lambda_R$	1
			-4/3	$e_R^- d_L \rightarrow \ell^- d$	λ_R	1				+5/3	$e_L^+ u_L \rightarrow \ell^+ u$	λ_R	1
$\tilde{V}_{1/2}^L$	1	2	-1/3	$e_L^- u_R \rightarrow \ell^- u$	λ_L	1	$\tilde{S}_{1/2}^L$	0	0	+2/3	$e_R^+ d_R \rightarrow \ell^+ d$	λ_L	1

- Limits based on running for 5 years with instantaneous luminosity of $\mathcal{L} \sim 10^{38} \text{ cm}^{-2} \text{ s}^{-1}$

- Positron beam polarization varied between:

$$P_e = [-80\%, 80\%]$$

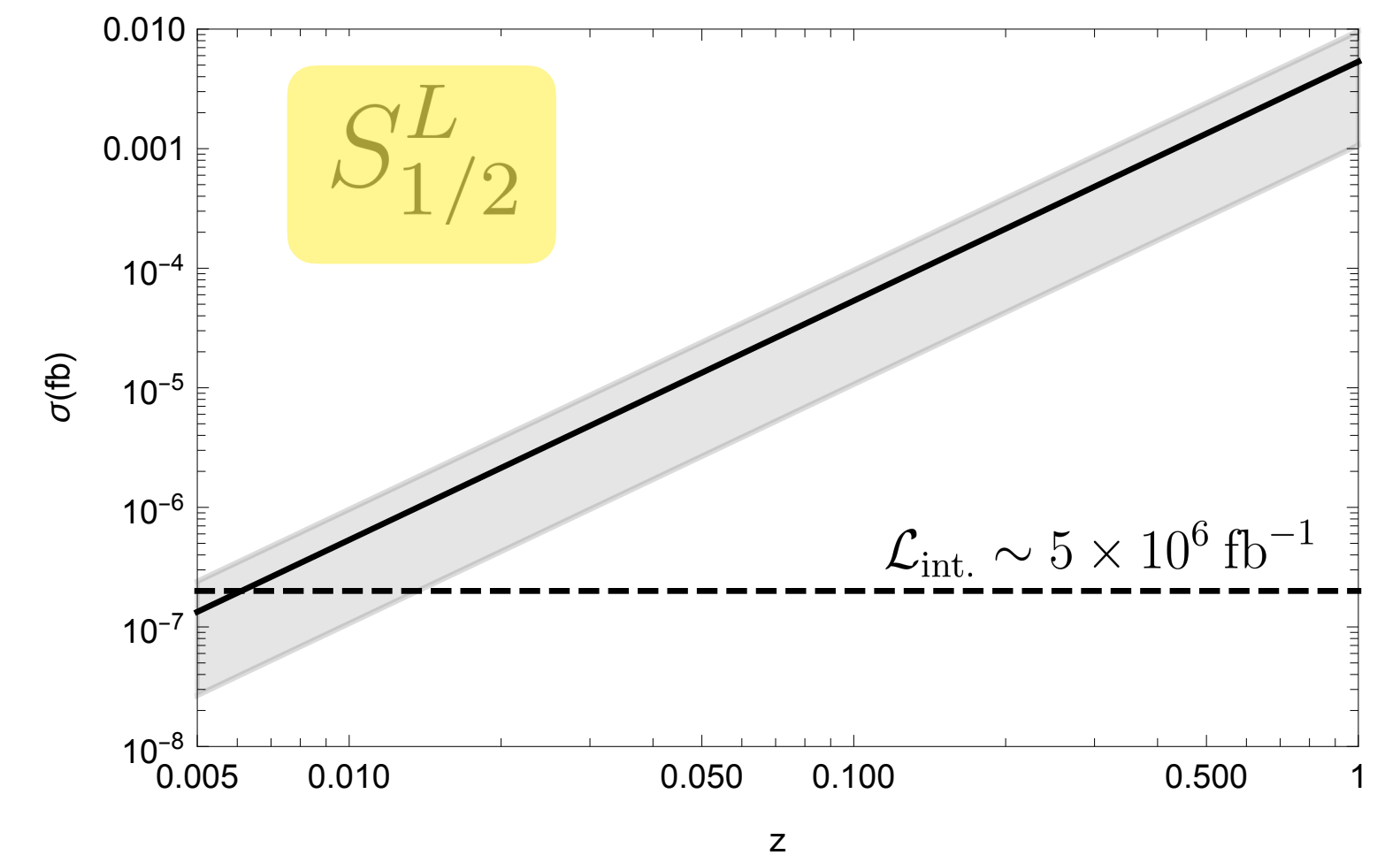
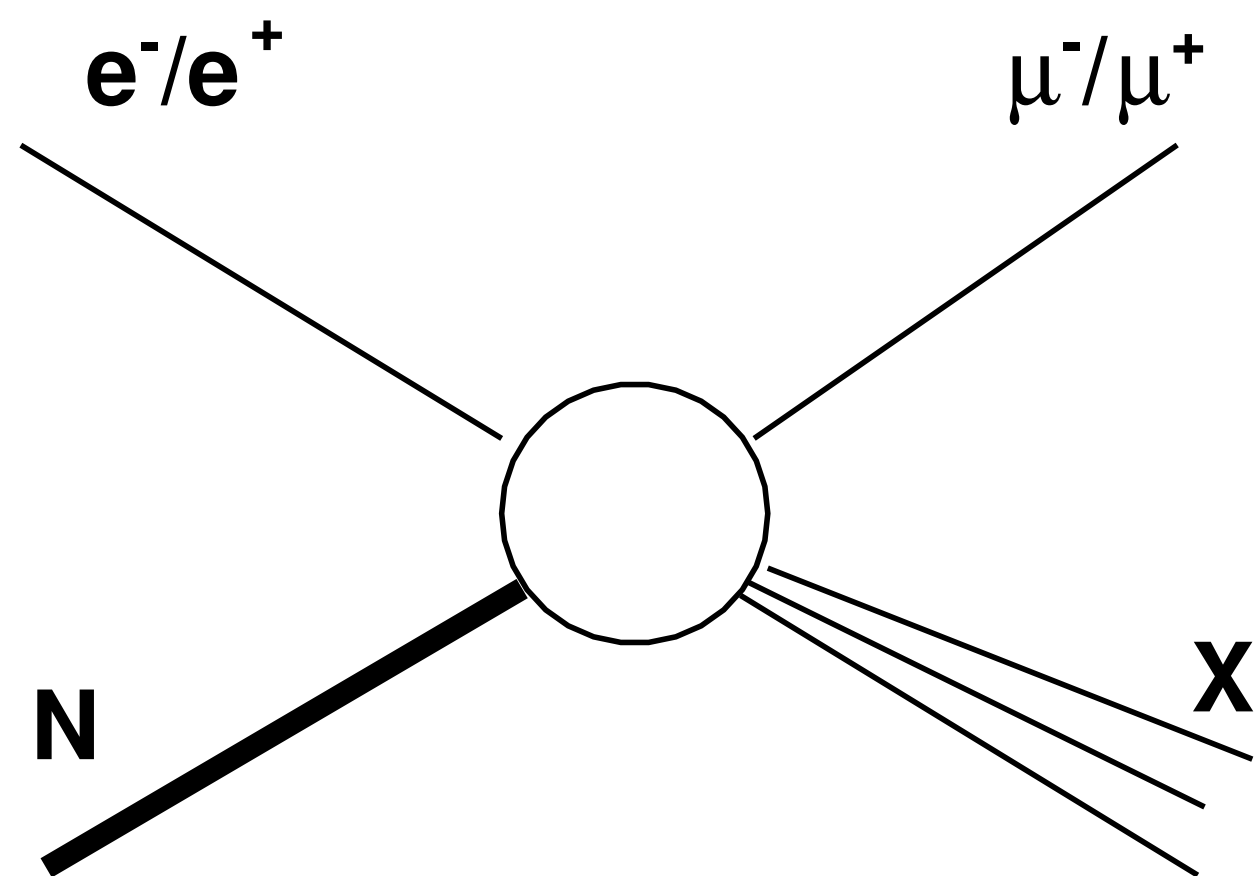


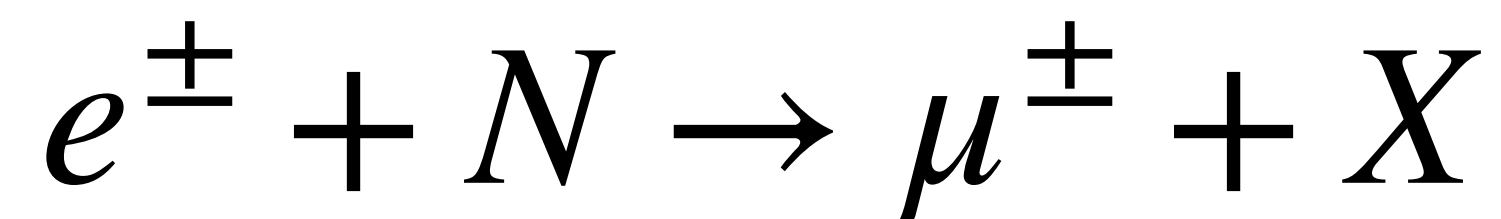
Fig. 6. The positron beam polarization dependence of cross section for $e^+ N \rightarrow \mu^+ X$ with center of mass energy $\sqrt{s} = 4.5$ GeV, via exchange of the $F=0$ scalar LQ, $S_{1/2}^L$, as a function of the ratio z defined in Eq. (9). The solid black line corresponds to the cross section for an unpolarized positron beam ($P_e = 0$). The gray band corresponds to the linear variation of the cross section with beam polarization, as shown in Eq. (11). The size of the band corresponds to a variation of the beam polarization between $[-80\%, 80\%]$.

Experimental Considerations



$$\sqrt{s} = 4.5 \text{ GeV}$$

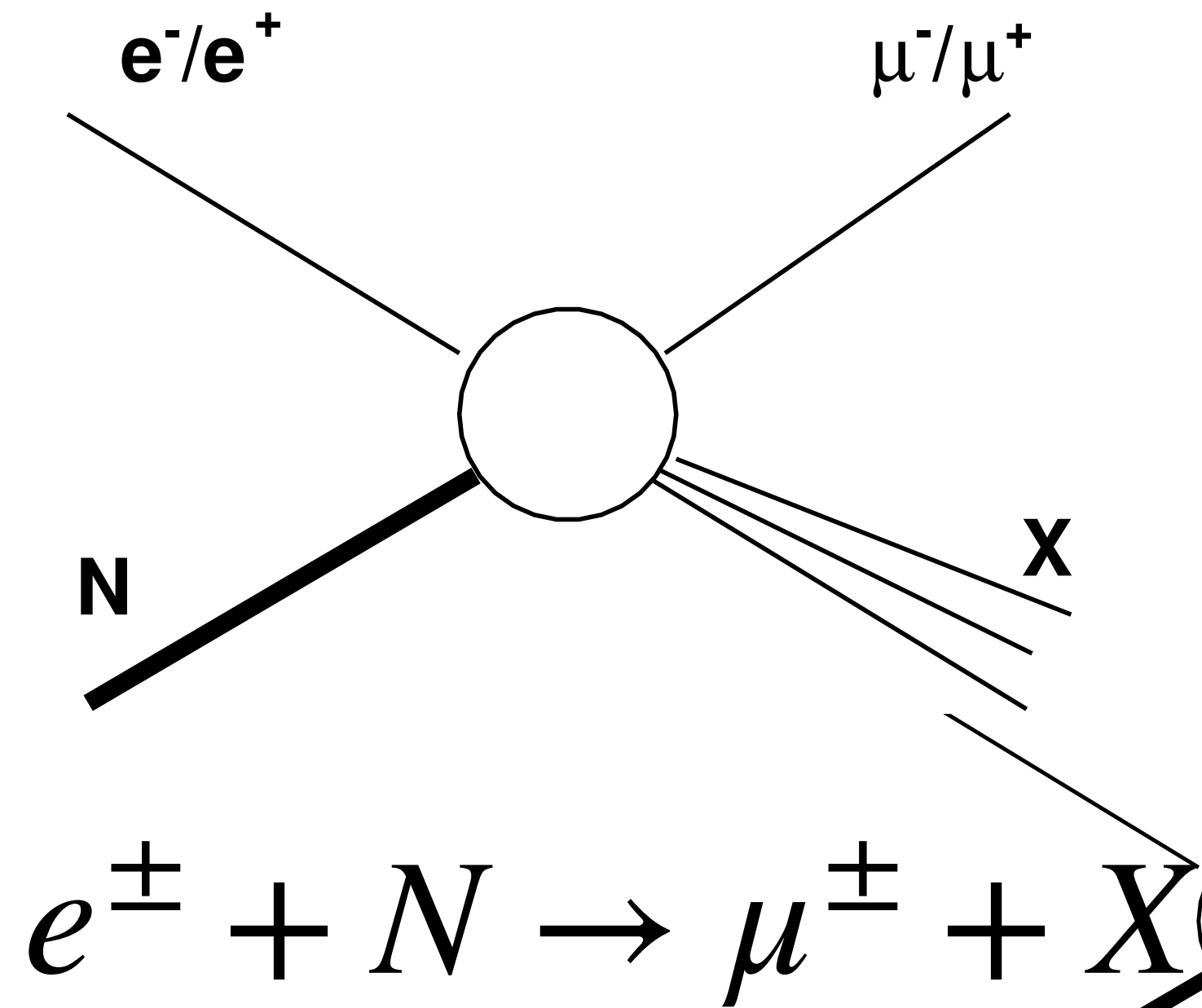
$$\mathcal{L} = 10^{36-39} \text{ cm}^{-2} \text{ s}^{-1}$$



- Required experimental capabilities:

- good muon detectors
- good charged particle tracking
- good vertex resolution

SoLID Experiment



$$\sqrt{s} = 4.5 \text{ GeV}$$

$$\mathcal{L} = 10^{36-39} \text{ cm}^{-2} \text{ s}^{-1}$$

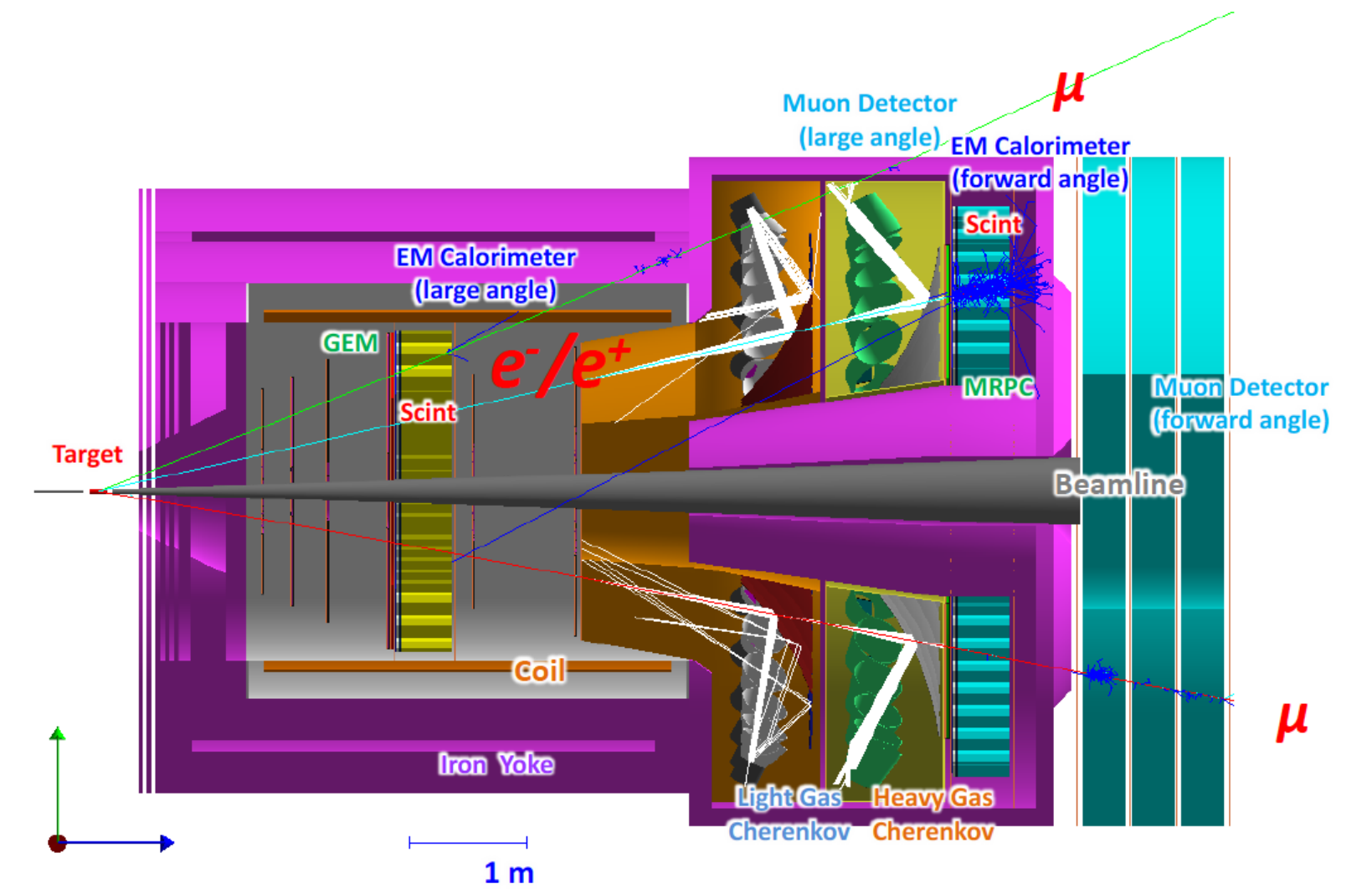


Fig. 3. The SoLID J/ψ configuration with muon detectors [28]. Other sub-detectors are labeled.

- Polar angle acceptance:

SIDIS configuration : $\theta = [8^\circ, 24^\circ]$

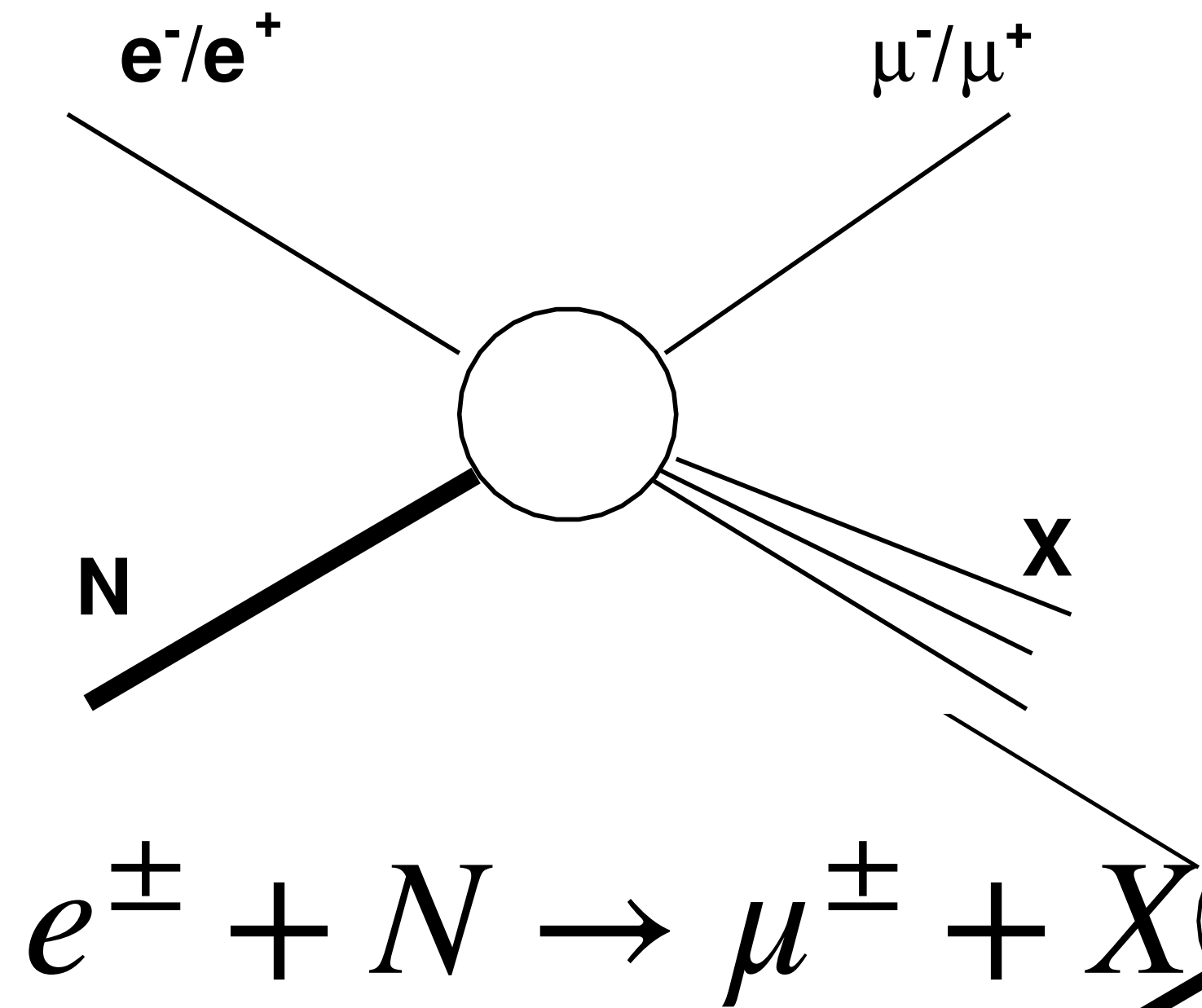
PVDIS configuration : $\theta = [22^\circ, 35^\circ]$

- Azimuthal angle acceptance:

full- 2π acceptance

Most of the cross section is in the forward region due to the kinematic boost of a 11 GeV lepton beam.

SoLID Experiment



$$\sqrt{s} = 4.5 \text{ GeV}$$

$$\mathcal{L} = 10^{36-39} \text{ cm}^{-2} \text{ s}^{-1}$$

- Muon Chambers:

The J/ψ and DDVCS configurations will be equipped with muon chambers

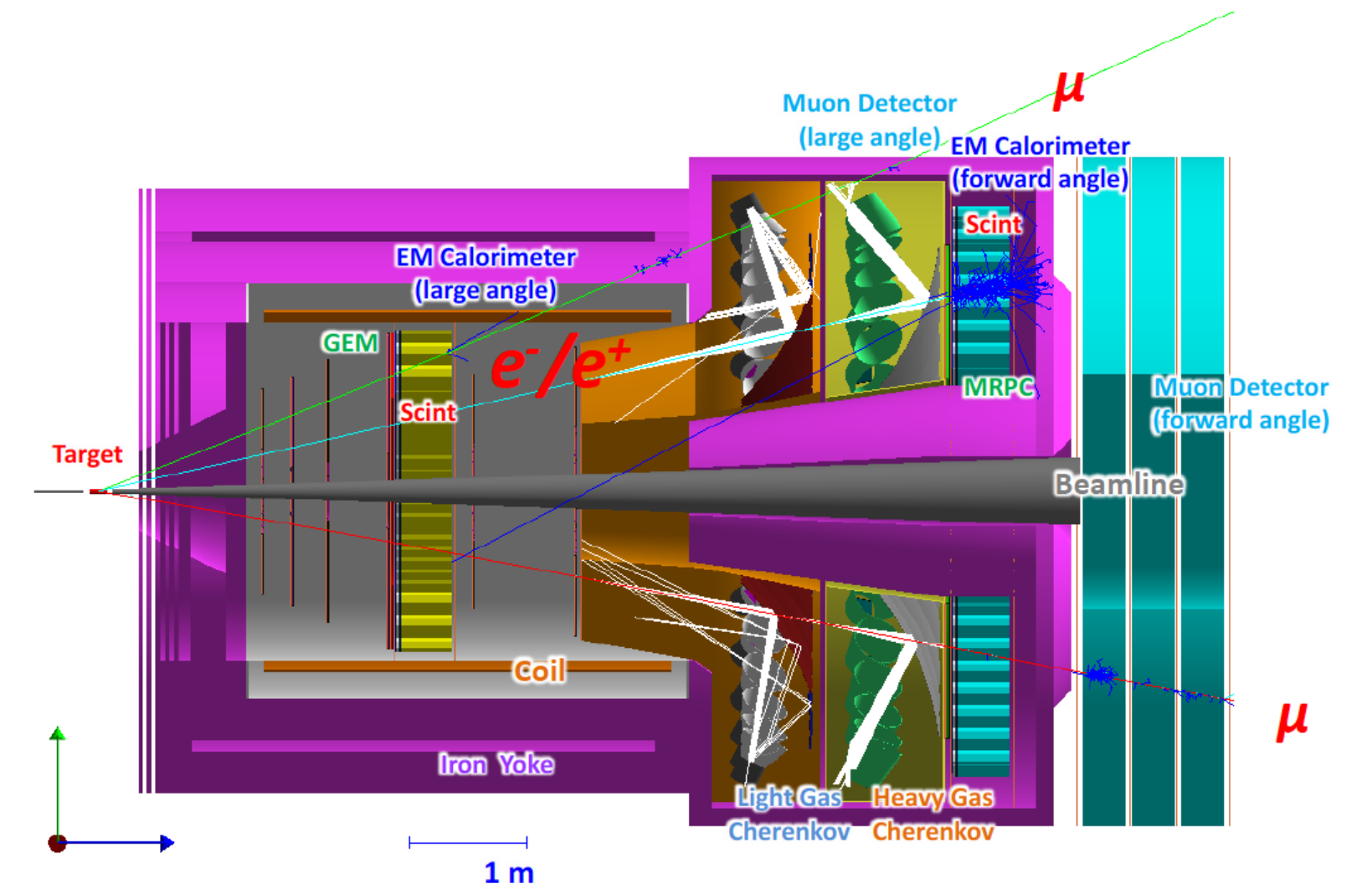
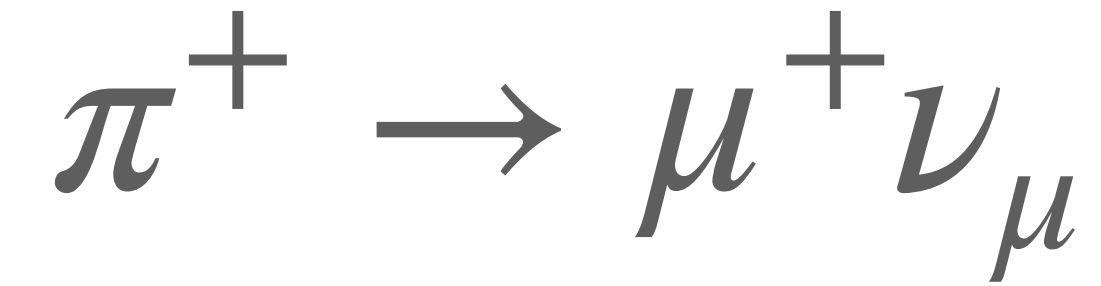


Fig. 3. The SoLID J/ψ configuration with muon detectors [28]. Other sub-detectors are labeled.

Muon Backgrounds

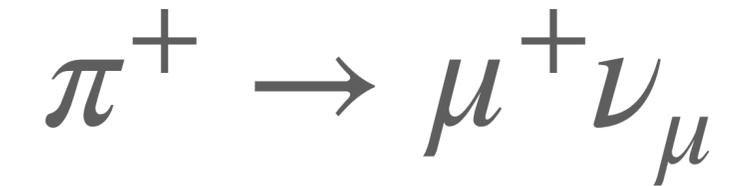
- The dominant background to the CLFV signal muon will come from decays of pions to muons:



- This background will be suppressed due to the compact size of the SoLID detector, so that the typical pion decay length is much bigger than the distance to the detector from their production vertex.

Muon Backgrounds

- The dominant background to the CLFV signal muon will come from decays of pions to muons:

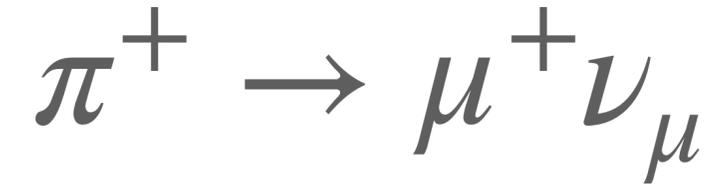


- This background will be suppressed due to the compact size of the SoLID detector, so that the typical pion decay length is much bigger than the distance to the detector from their production vertex.

$$P(L) = e^{-L/\lambda_D^{\pi}}, \quad \lambda_D^{\pi} = \frac{p_{\pi}}{m_{\pi}c} c\tau,$$

Muon Backgrounds

- The dominant background to the CLFV signal muon will come from decays of pions to muons:



- This background will be suppressed due to the compact size of the SoLID detector, so that the typical pion decay length is much bigger than the distance to the detector from their production vertex.

$$P(L) = e^{-L/\lambda_D^\pi}, \quad \lambda_D^\pi = \frac{p_\pi}{m_\pi c} c\tau,$$

- Pions will be typically produced with momenta in the range:

$$1 \text{ GeV} \lesssim p_\pi \lesssim 7 \text{ GeV}$$

- Thus, the typical pion decay lengths will be in the range:

$$56 \text{ m} \lesssim \lambda_D^\pi \lesssim 390 \text{ m}$$

(Pion decay length)

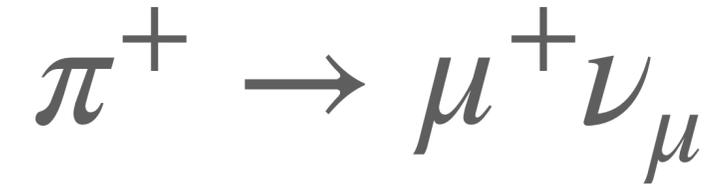
\gg

$$\sim 5 \text{ m}$$

(Overall detector dimensions,
combined with proximity to
pion production vertex)

Muon Backgrounds

- The dominant background to the CLFV signal muon will come from decays of pions to muons:



- This background will be suppressed due to the compact size of the SoLID detector, so that the typical pion decay length is much bigger than the distance to the detector from their production vertex.

$$P(L) = e^{-L/\lambda_D^\pi}, \quad \lambda_D^\pi = \frac{p_\pi}{m_\pi c} c\tau,$$

- Pions will be typically produced with momenta in the range:

$$1 \text{ GeV} \lesssim p_\pi \lesssim 7 \text{ GeV}$$

- Thus, the typical pion decay lengths will be in the range:

$$56 \text{ m} \lesssim \lambda_D^\pi \lesssim 390 \text{ m} \quad \gg \quad \sim 5 \text{ m}$$

(Pion decay length)

(Overall detector dimensions,
combined with proximity to
pion production vertex)

- Correspondingly, the pion survival probability at the detector is:

$$p_\pi \sim 1 \text{ GeV} \rightarrow 91 \% \text{ survival probability}$$

$$p_\pi \sim 7 \text{ GeV} \rightarrow 99 \% \text{ survival probability}$$

Muon Backgrounds

- Charged particle tracking spatial resolution of 100 microns, allowing for precise reconstruction of pion decay vertices to further suppress backgrounds.:
- Other backgrounds can arise from charmed meson decays or J/ψ decays. Once again tracking and vertex resolution capabilities can help suppress such backgrounds.
- Due to the small center of mass energy, $\sqrt{s} \sim 4.5$ GeV, there are no backgrounds from B-meson decays.

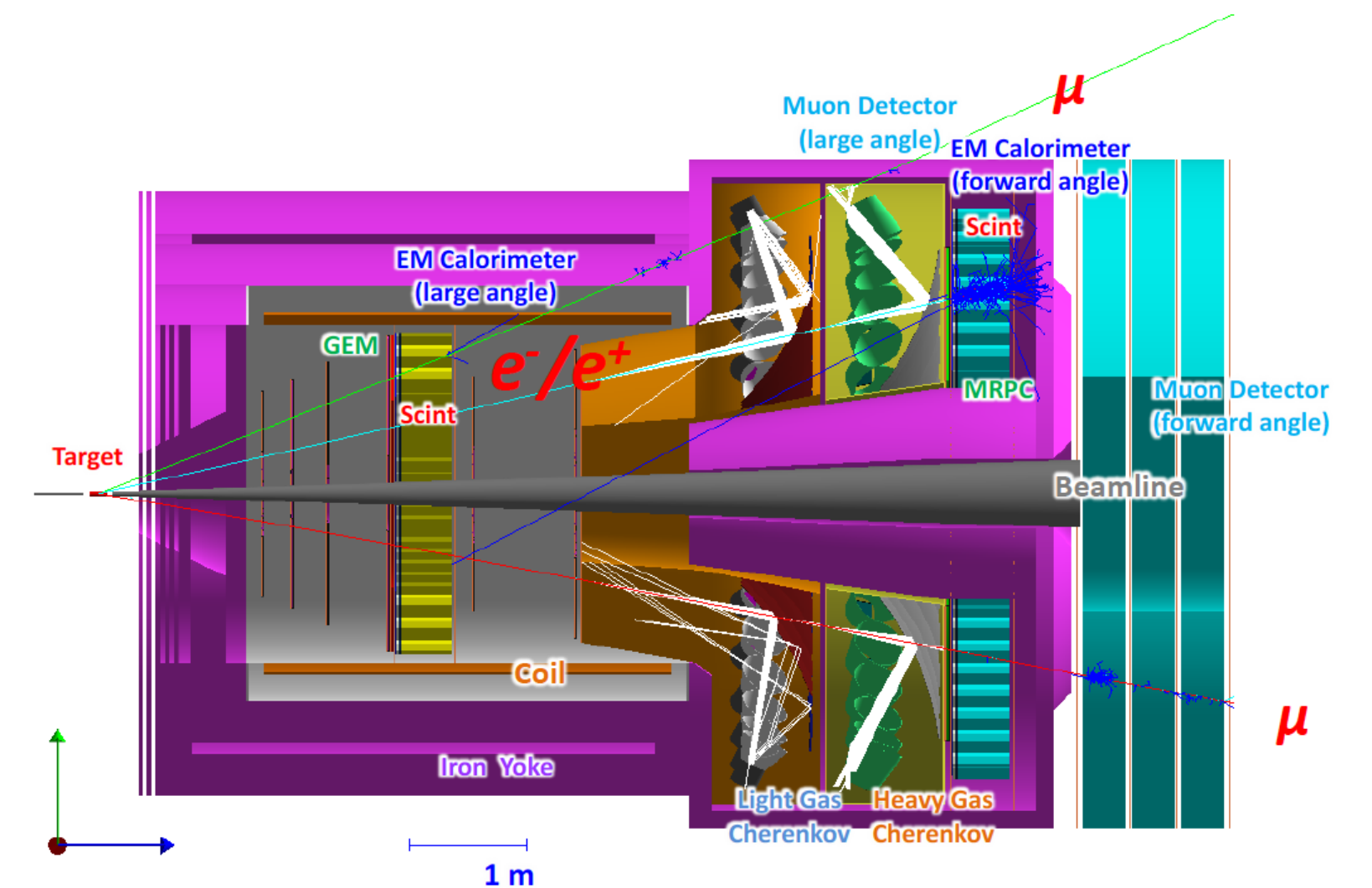


Fig. 3. The SoLID J/ψ configuration with muon detectors [28]. Other sub-detectors are labeled.

More detailed simulation studies needed to estimate the impact of acceptance and backgrounds on CLFV limits.

Conclusions

- The high luminosity and acceptance of SoLID can allow for a significant improvement on HERA limits in the CLFV process:

$$e^{\pm} + N \rightarrow \mu^{\pm} + X$$

- A positron beam will be complementary to an electron beam for disentangling different possible CLFV mechanisms.
- Detectors should be equipped with muon detectors and good tracking. SoLID has these capabilities.
- Muon backgrounds must be well-understood and under control.
- Detailed simulation studies needed to fully assess the impact of acceptance and background on CLFV limits.